THE DARK ENERGY SURVEY IMAGE PROCESSING PIPELINE

E. Morganson[1,2], R. A. Gruendl[1,2], F. Menanteau[1,2], M. Carrasco Kind[1,2], Y.-C. Chen[1,2], G. Daues[1],
A. Drlica-Wagner[3], D. N. Friedel[1,2], M. Gower[1], M. W. G. Johnson[1], M. D. Johnson[1], R. Kessler[4], F. Paz-Chinchón[1,2],
D. Petravick[1], C. Pond[1], B. Yanny[3], S. Allam[3], R. Armstrong[5], W. Barkhouse[6], K. Bechtol[7], A. Benoit-Lévy[8,9,10],
G. M. Bernstein[11], E. Bertin[8,10], E. Buckley-Geer[3], R. Covarrubias[1], S. Desai[12], H. T. Diehl[3], D. A. Goldstein[13,14],
D. Gruen[15,16], T. S. Li[3], H. Lin[3], J. Marriner[3], J. J. Mohr[17,18,19], E. Neilsen[3], C.-C. Ngeow[20], K. Paech[17,21],
E. S. Rykoff[15,16], M. Sako[11], I. Sevilla-Noarbe[22], E. Sheldon[23], F. Sobreira[24,25], D. L. Tucker[3], W. Wester[3]

(DES Collaboration)

[1] National Center for Supercomputing Applications, University of Illinois at Urbana-Champaign, 1205 West Clark St., Urbana, IL 61801, USA
[2] Department of Astronomy, University of Illinois at Urbana-Champaign, 1002 W. Green Street, Urbana, IL 61801, USA
[3] Fermi National Accelerator Laboratory, P. O. Box 500, Batavia, IL 60510, USA
[4] Kavli Institute for Cosmological Physics, University of Chicago, Chicago, IL 60637, USA
[5] Department of Astrophysical Sciences, Princeton University, Peyton Hall, Princeton, NJ 08544, USA
[6] University of North Dakota, Department of Physics and Astrophysics, Witmer Hall, Grand Forks, ND 58202, USA
[7] LSST, 933 North Cherry Avenue, Tucson, AZ 85721, USA
[8] CNRS, UMR 7095, Institut d'Astrophysique de Paris, F-75014, Paris, France
[9] Department of Physics & Astronomy, University College London, Gower Street, London, WC1E 6BT, UK
[10] Sorbonne Universités, UPMC Univ Paris 06, UMR 7095, Institut d'Astrophysique de Paris, F-75014, Paris, France
[11] Department of Physics and Astronomy, University of Pennsylvania, Philadelphia, PA 19104, USA
[12] Department of Physics, IIT Hyderabad, Kandi, Telangana 502285, India
[13] Department of Astronomy, University of California, Berkeley, 501 Campbell Hall, Berkeley, CA 94720, USA
[14] Lawrence Berkeley National Laboratory, 1 Cyclotron Road, Berkeley, CA 94720, USA
[15] Kavli Institute for Particle Astrophysics & Cosmology, P. O. Box 2450, Stanford University, Stanford, CA 94305, USA
[16] SLAC National Accelerator Laboratory, Menlo Park, CA 94025, USA
[17] Excellence Cluster Universe, Boltzmannstr. 2, 85748 Garching, Germany
[18] Faculty of Physics, Ludwig-Maximilians-Universität, Scheinerstr. 1, 81679 Munich, Germany
[19] Max Planck Institute for Extraterrestrial Physics, Giessenbachstrasse, 85748 Garching, Germany
[20] Graduate Institute of Astronomy, National Central University, Jhongli 32001, Taiwan
[21] Universitäts-Sternwarte, Fakultät für Physik, Ludwig-Maximilians Universität München, Scheinerstr. 1, 81679 München, Germany
[22] Centro de Investigaciones Energéticas, Medioambientales y Tecnológicas (CIEMAT), Madrid, Spain
[23] Brookhaven National Laboratory, Bldg 510, Upton, NY 11973, USA
[24] Instituto de Física Gleb Wataghin, Universidade Estadual de Campinas, 13083-859, Campinas, SP, Brazil
[25] Laboratório Interinstitucional de e-Astronomia - LIneA, Rua Gal. José Cristino 77, Rio de Janeiro, RJ - 20921-400, Brazil

Draft version January 11, 2018

ABSTRACT

The Dark Energy Survey (DES) is a five-year optical imaging campaign with the goal of understanding the origin of cosmic acceleration. DES performs a ~ 5000 deg^2 survey of the southern sky in five optical bands (g,r,i,z,Y) to a depth of $\sim$24th magnitude. Contemporaneously, DES performs a deep, time-domain survey in four optical bands (g,r,i,z) over ~ 27 deg^2. DES exposures are processed nightly with an evolving data reduction pipeline and evaluated for image quality to determine if they need to be retaken. Difference imaging and transient source detection are also performed in the time domain component nightly. On a bi-annual basis, DES exposures are reprocessed with a refined pipeline and coadded to maximize imaging depth. Here we describe the DES image processing pipeline in support of DES science, as a reference for users of archival DES data, and as a guide for future astronomical surveys.

Keywords: surveys, catalogs, techniques: image processing, techniques: photometric, cosmology: observations

1. INTRODUCTION

The Dark Energy Survey (DES) is a large optical imaging survey designed to improve our understanding of the origin of cosmic acceleration and the nature of dark energy using four complementary methods: weak gravitational lensing, galaxy cluster counts, the large-scale clustering of galaxy (including baryon acoustic oscillations), and distances to Type Ia supernova (DES Collaboration 2005). DES uses the 3 deg^2 Dark Energy Camera (DECam; Flaugher et al. 2015), a 570 Megapixel camera installed at prime focus on the Blanco 4-m telescope at the Cerro Tololo Inter-American Observatory (CTIO) in northern Chile. Each exposure travels from CTIO

to the National Optical Astronomical Observatory (NOAO) for archiving and then to the National Center for Supercomputing Applications (NCSA) at the University of Illinois at Urbana-Champaign for processing within minutes of being observed.

DES began in August 2013 and observes for roughly six months out of the year (August through mid-February). DECam Science Verification (SV) data were taken between 2012 November 1 and 2013 February 22 were of sufficient quality to be included in some DES data sets. Raw exposures are publicly available from NOAO one year after acquisition, and DES is scheduled to provide two public releases of processed

data.[1]

DES is one in a series of large optical surveys that includes the Sloan Digital Sky Survey (SDSS; York et al. 2000), the Panoramic Survey Telescope and Rapid Response System 1 (Pan-STARRS1 or PS1; Kaiser et al. 2010), Kilo Degree Survey (KiDS; de Jong et al. 2013), the Hyper Suprime-Cam SSP Survey (HSC; Aihara et al. 2017) and the future Large Survey Synoptic Telescope (LSST; Ivezic et al. 2008). DES comprises two multi-band imaging surveys: a $\sim 5000 \deg^2$ wide-area survey of the southern sky in the g, r, i, z and Y bands and a survey of $\sim 27 \deg^2$ observed with high cadence in the g, r, i and z bands to detect supernovae and characterize their light curves. The DES filters are very similar to their analogously-named counterparts from other surveys. Uniquely, the DES z band extends redward of, for instance, the SDSS z band and largely overlaps with the DES Y band (Figure 1). DECam also has a near ultraviolet u filter, a wide optical VR filter, and a narrow $N964$ filter. None of these are used directly by DES, although some supplemental u-band data has been taken in the DES supernova fields and elsewhere.

The DES wide-area survey footprint covers $\sim 5000 \deg^2$ of the southern Galactic cap (Fig. 2), overlapping SDSS Stripe 82 along the celestial equator and $\sim 2500 \deg^2$ of South Pole Telescope footprint (Carlstrom et al. 2011). The DES wide-area survey images have a nominal 10σ limiting magnitudes of $g = 23.57$, $r = 23.34$, $i = 22.78$, $z = 22.10$ and $Y = 20.69$.[2] The final coadded depth will be roughly one magnitude deeper. DES wide-area images have a median seeing of $\sim 0.''99$.

To accomplish the DES scientific goals, the DES Data Management system (DESDM, Ngeow et al. 2006, Mohr et al. 2008, Sevilla et al. 2011, Mohr et al. 2012, Desai et al. 2012) generates a variety of scientific products. For the DES wide-area survey, DESDM produces reduced single-epoch images, deeper coadded images, and catalogs of suitable quality to perform photometric redshift, weak lensing, and other precise analyses. DESDM produces difference images and catalogs for each observation of a supernova field. In addition to facilitating the cosmological analyses that primarily motivated DES, these data products will provide a rich legacy for the astronomical community (DES Collaboration 2016).

The processing pipeline described here was first applied to a cumulative processing of data from Year 1 (Y1) through Year 3 (Y3), and serves as the foundation of the first DES public data release (DES DR1; DES Collaboration 2018). This pipeline differs somewhat from that used to create the Y1A1 data products Drlica-Wagner et al. (2017) and the associated Y1A1 GOLD catalog used for DES Y1 cosmology results (e.g., DES Collaboration 2017 and associated papers). We attempt to describe places where the two pipelines differ appreciably.
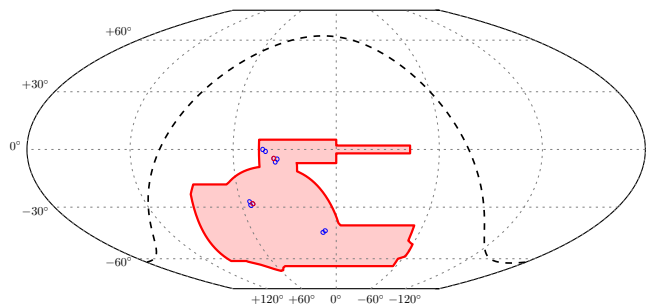
We document here how the DES data products, processed images and catalogs, are generated from raw DECam images. In the next section, we summarize the flow of data from the camera through our processing pipelines. In Section 3, we describe the preprocessing: generating image calibration data and handling camera-based artifacts. Section 4 describes the First Cut pipeline, the nightly processing of wide-area data
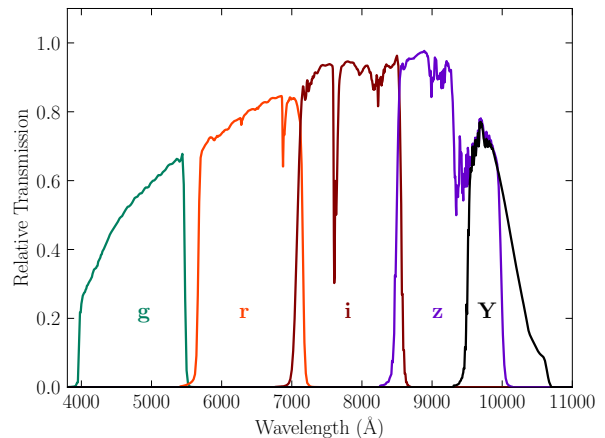
Figure 1. The DES g, r, i, z and Y Standard Bandpasses. These curves include atmospheric transmission and instrumental response. Details can be found in Burke et al. (2018).
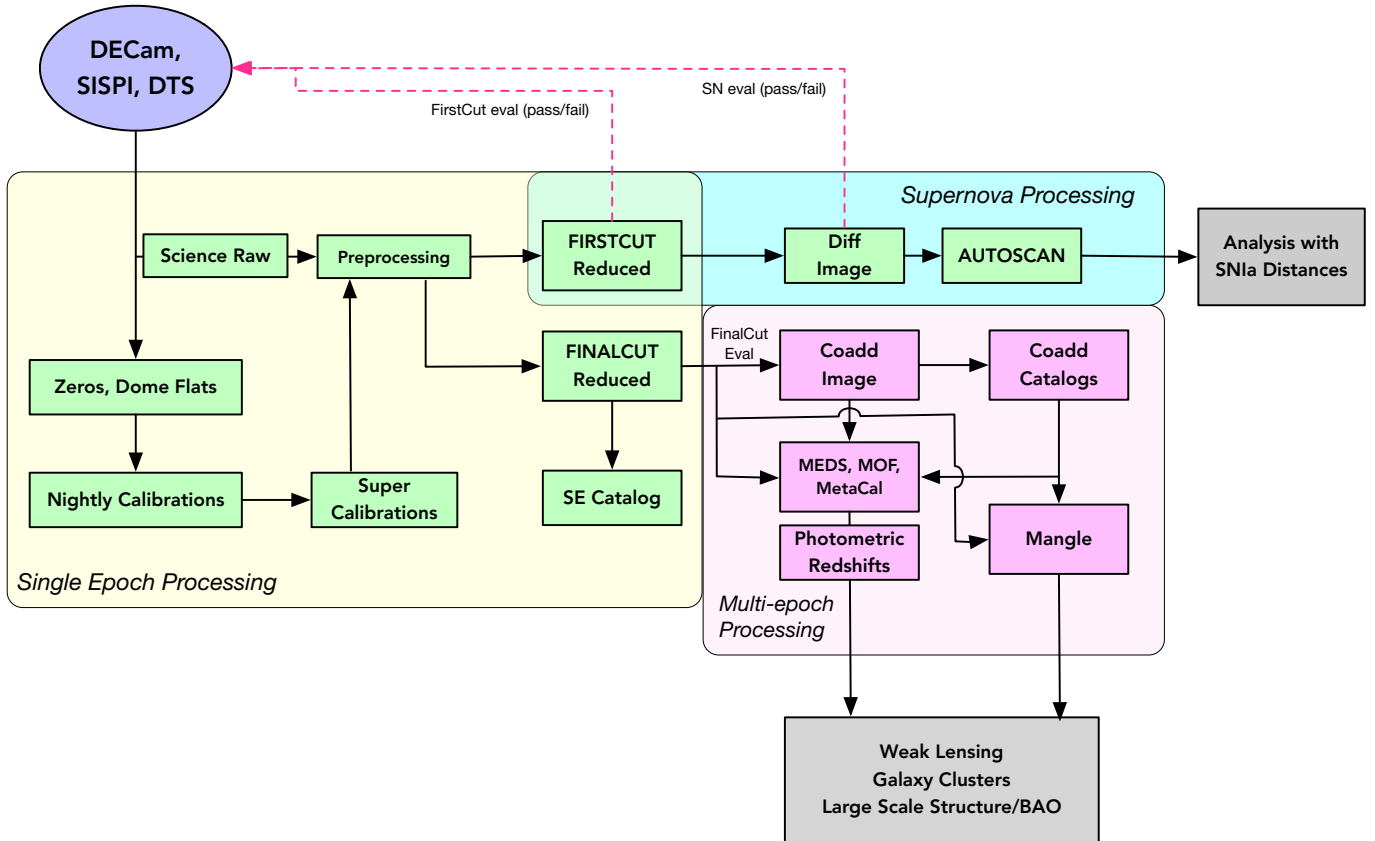

Figure 2. An equal-area McBryde-Thomas flat-polar quartic projection of the DES footprint in celestial equatorial coordinates. The main 5000 deg^2 survey footprint for DES is shown in red. The 8 shallow supernova fields are shown as blue circles, and the 2 deep supernova fields are shown as red circles. The Milky Way plane is shown as a dashed line.

primarily used for data assessment, and the minor changes we made for our "Final Cut" processing for public release. Section 5 describes our nightly supernova processing. We describe our Multi-Epoch pipeline, which includes coaddition of images and more precise photometry, in Section 6.

2. DATA FLOW

In this section we provide a high-level overview of the DES data flow starting with mountain-top observations and concluding with final processed data products (Fig. 3). DES observations are scheduled by the Observer Tactician software (OBSTAC; Neilsen & Annis 2013), which determines the on-sky observing strategy based on observing conditions and current survey needs using data quality assessments from previously processed data. Our 10 supernova fields are observed every seven days or when the seeing exceeds $1.''1$. After each observation, the Survey Image System Process Integration (SISPI; Honscheid et al. 2012) transfers the raw exposures to the NOAO via the Data Transport System (DTS; Fitzpatrick 2010) for archiving. Exposures continue from NOAO to the National Center for Supercomputing Applications (NCSA) for processing. Calibration images (bias, dark, and dome flat exposures) are delivered nightly and processed into the format used for flat fielding (Section 3.2).

The DES data are collected by DECam, a 570 Megapixel camera at the Blanco 4-m telescope at the CTIO in Chile. The DECam focal plane is comprised of 62 science CCDs

---

[1] https://des.ncsa.illinois.edu/releases

[2] Limiting magnitudes were calculated from the median PSF magnitude of all sources with S/N = 10 detected in exposures taken under nominal observing conditions. These estimates of the limiting magnitudes have an RMS spread of roughly ±0.09 mag.

Figure 3. A schematic view of the modules and steps involved in the DESDM Pipeline. Calibration and raw science images are delivered from DECam by SISPI and DTS to NCSA. In Single Epoch Processing (yellow box), raw science exposures undergo preprocessing and are combined with calibration images to produce First Cut images for initial inspection and Final Cut images for science releases. Images in the Supernova fields are processed with the Supernova Pipeline (blue boxes). Final Cut images and catalogs are sent to Multi-Epoch Processing (pink box), the outputs of which go to the science groups for validation and analysis (gray boxes). The science pipelines are not described in this paper.

(see Fig. 4) which are each readout by two amplifiers. DECam has 8 additional corner CCDs for guiding, focusing and alignment. These 8 CCDs are not reduced or analyzed in our pipelines. In addition, the routines described here are not used to process CCD 61, which failed in 2012. Similarly, CCD 2 was not processed between November 2013 and December 2016, during which time it was not functional. Amplifier A of CCD 31 has an unpredictable, time-variable gain and is not processed or used for DES science. Amplifier B of CCD 31 functions normally and is processed. The rest of the science CCDs are performing within specifications and are usable for science. Thus, we have used either 59.5 or 60.5 CCDs throughout most of the survey. Each science CCD has 2048×4096 pixels and the pixel scale varies smoothly from $0.''2636$ per pixel down to $0.''2626$ per pixel as one travels from the center of the camera focal plane out to its edge, 1.1 degrees away. The total active area covered by all science CCDs is roughly $2.7 \deg^2$. Each DECam amplifier is readout with a virtual overscan comprising 6 pre-scan pixels at the beginning of each row and 50 overscan pixels at the end of each row. The DECam CCDs are readout at a pixel rate of 250 kHz (per amplifier) setting an overall readout time of 17 seconds. This readout time is less than the typical overhead and slewing time between exposures.

DES has both a wide-area and a supernova component. These different survey components require different exposure times, described in Table 1. In the wide-area survey, expo-

Filter	Wide field	Shallow Supernova	Deep Supernova
g	90	175	200×3
r	90	150	400×3
i	90	200	360×5
z	90	200×2	330×11
Y	45/90	–	–

Table 1
Exposure times (in seconds) for DES wide-area and supernova exposures. Deep Supernova fields and the Shallow Supernova field z-band images are constructed of multiple exposure "coadds", and we note the number of exposures as appropriate. In Y4, the Y-band exposure time went from 45 seconds to 90 seconds.

sures are 90 seconds in the g, r, i and z bands, and the 5-year survey goal is to obtain 10 exposures in each band. Initially, DES planned to obtain ten 45 second exposures in the Y band, but in Y4 DES began collecting one 90 second exposure per year to reduce overhead. The total exposure time should be 900 seconds in the g, r, i and z bands and 450 seconds in the Y band. To optimize for supernova detection, the ten supernova fields are observed to the same limiting magnitude depth in the g, r, i and z bands. This optimization requires longer exposure time in the redder bands as described in Table 1. We will ultimately visit each supernova field 120 times, providing total exposure times much longer than the wide-area survey.

DES wide-area data are processed with the First Cut pipeline (Section 4). Wide-area exposures are typically pro-
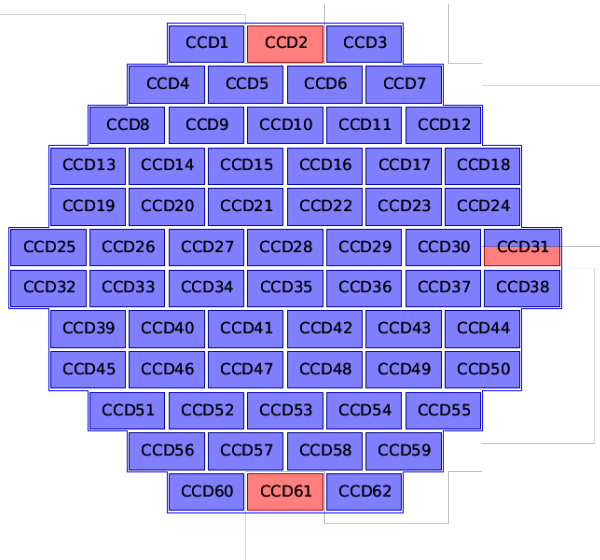
Figure 4. DECam focal plain chips layout. Each of the 62 rectangles represents a CCD which is in turn read by two amplifiers (along the long direction). CCDs 2 and 61 have been inactive for most of DES. Amplifier A of CCD 31 has unpredictable gain and has not been processed by DES. These areas are marked in red.

cessed within 10 hours of being taken, which allows for rapid evaluation of data quality (Section 4.7). The supernova pipeline (Section 5) begins by processing images identically to the First Cut pipeline. It then produces a difference image with the nightly image and a previously generated template to identify transient events. The supernova data are given higher priority in our processing queue to ensure that they are processed and evaluated before the subsequent night. The goal of the First Cut pipeline is to determine whether or not an exposure meets survey quality requirements for image quality and image depth (Section 4.7). Supernova processing has an analogous image evaluation procedure (Section 5.7). If an exposure does not satisfy the data quality criteria for the relevant survey, then that field-band combination is placed back on the stack for observation. Data evaluations are usually completed before the start of observing the following night.

The single epoch images are processed multiple times. The aforementioned First Cut pipeline is run immediately for image evaluation. Final Cut processing occurs at the end of a season, typically in March, and is a full reprocessing of all the single epoch exposure from the prior 6 months. The Final Cut processing uses carefully constructed calibration images for flat fielding and sky characterization (see Section 4.8) and a single pipeline that includes all improvements developed during the observing season. A rough photometric calibration ($\approx$ 5% RMS scatter) is performed by the pipelines above. More precise zeropoints are assigned to the Final Cut data with the calibration procedure described in Burke et al. (2018).

After Final Cut, we employ a Multi-Epoch pipeline to maximize survey depth by coadding images into a single wide-area image (Section 6). We create a catalog of astronomical objects from these images. We also produce depth maps which are used to model survey depth as a function of position on the sky using MANGLE (Hamilton & Tegmark 2004, Swanson et al. 2008) and produce Multi Epoch Data Structure (MEDS; Jarvis et al. 2015) postage stamps of every object. We then perform improved photometric and morphological measurement with multi-epoch, multi-object fitting (MOF; Drlica-Wagner et al. 2017), and Metacalibration (Metacal;

Sheldon & Huff 2017), a technique to accurately measure weak gravitational lensing shear. After source detection and measurement, the DES data are ready to be analyzed by high-level science algorithms.

Over the first four years of the survey (i.e. as of 2017 June 15), DES has taken 67130 wide-area exposures and 9571 supernova exposures. We anticipate $\sim$85000 and $\sim$12000 wide-area and supernova exposures when the survey is complete. This excludes photometric calibration and astrometric alignment images. The average raw exposure (compressed losslessly by a factor of roughly 2) is 0.47 GB, and we have processed 36 TB of raw science data. This expands to 128 TB if we include calibration images and other ancillary data, and balloons to 1.0 PB of processed image and catalog products. The wide-area survey and supernova images comprise 1510 hours and 680 hours of DECam time, respectively. Each reprocessing of the wide-area data requires roughly 500,000 core hours. The more intensive supernova processing, which includes difference imaging, requires 600,000 core hours. In addition, DESDM used 200,000 core hours to process 10,346 coadded tiles. Including all reprocessing campaigns, DESDM has used roughly 2 million core hours at a combination of the test cluster at NERSC, NCSA's iForge cluster, Fermilab's Fermigrid batch computing system (Chadwick et al. 2008), the University of Illinois campus cluster and the Blue Waters supercomputer (Bode et al. 2013). We use Oracle Real Application Cluster 12c to support development, testing, nightly operations, data release production, and data distribution. The total size of the processing database (containing processing log information) and the science release database (containing objects catalogs) are currently 36 TB and 17 TB, respectively.
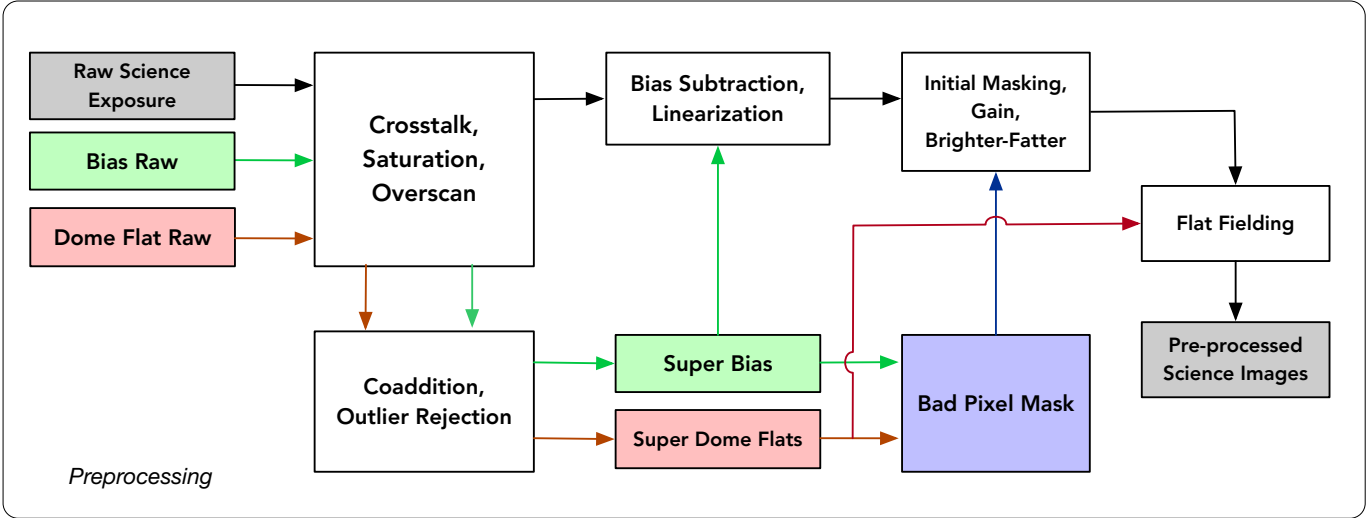
3. PREPROCESSING

All raw DECam exposures require a set of generic corrections before image-specific processing. We call these routines "Preprocessing" and diagram them in Fig. 5, a zoom in of the Preprocessing box from Fig. 3. These procedures include crosstalk correction, bias subtraction, bad pixel masking (masking known problematic pixels in the camera), correcting nonlinear pixel response, and flat fielding. These corrections in turn require a series of engineering tables for crosstalk and linearization, as well as bias images, dome flats, star flats, bad pixel masks and sky background model images. We describe our preprocessing routines, tables and images below. Additional flat-fielding routines are performed later in the processing in Section 4.3. Many of the underlying phenomena here have their mathematical and physical basis described in detail in Bernstein et al. (2017).

Preprocessing requires many auxiliary files and tables which we describe Table 6 and Table 7 of Appendix A. Table 6 lists, for each auxiliary correction element, the element's name, a brief description, how often the element is updated and which code module applies the element to the data during processing. Table 7 documents the bias and dome flat correction images, and also special tables and images to correct for other features such as non-linear CCD response. These auxiliary correction files and tables are referenced in Sections 3.2-4.3 below. Code to apply the correction images is publicly available.[3]

A DES "processing epoch" is declared at the beginning of each observing year, and also when an event, such as a camera warm-up/cool-down cycle, could change the characteris-

---

[3] https://github.com/DarkEnergySurvey

Figure 5. A diagram of the Preprocessing applied to every exposure. This is a "zoom in" of the the Preprocessing box in Fig. 3. This includes our initial masking and detrending with bias and flat images (green and red arrows, respectively). Preprocessed exposures are then processed with the First Cut or Final Cut pipeline.

Epoch Name	Begin Date	End Date
SVE1	2012.11.09	2013.02.22
Y1E1	2013.08.15	2013.11.28
Y1E2	2013.11.30	2014.02.12
Y2E1	2014.08.06	2014.11.30
Y2E2	2014.12.04	2015.05.18
Y3E1	2015.07.31	2016.02.23
Y4E1	2016.08.13	2016.12.31
Y4E2	2017.01.01	2017.02.18
Y5E1	2017.08.15	2017.09.04
Y5E2	2017.09.04	–

Table 2
A list of epoch names, begin dates and end dates. Date are in year.month.day format. The epochs are named for the survey year in which they were taken (with Science Verification data called SV) and then the epoch number within that year. So Y4E2 is the second epoch from the fourth year of the survey.

tics of the camera response (requiring new flat fields) or pixel-defect maps (new bad pixels appearing). Events that cause a significant change to the camera temperature can change the astrometry (relative orientation of the CCDs within the camera) by tiny amounts (a few microns), and can also change the flat field and other response of the camera by small amounts ($\ll$ 1%, but large enough to warrant generating a new set of auxiliary correction files). A list of processing epochs is shown in Table 2. Also, of note, baffling was added to reduce scattered light for the g band on 2013 April 22 and the other bands on 2013 August 12. The internal part of shutter and filter units were aerosolized (painted) on 2014 March 14.

3.1. *DECam Crosstalk*

Crosstalk occurs when the signal in one amplifier contaminates another. A crosstalk correction is generally necessary for any camera with multiple CCDs or amplifiers (Freyhammer et al. 2001). DES has measurable crosstalk between the two amplifiers on each CCD and sometimes between amplifiers on different CCDs. We correct for this crosstalk in both science exposures and all calibration images (Section 3.2).

DECam crosstalk was evaluated by comparing a series of images with bright stars randomly located across the focal plane. We correlate the flux that is measured by each "Source" amplifier on CCDs where the stars are imaged, to the flux measured for every other amplifier on the camera. Each other

amplifier is a potential "Victim", and we check for correlated charge measured in the pixel location that is read out simultaneously with the bright star. We fit for a linear coefficient to correct every Victim amplifier for "Source-Victim" combination:

$$\Delta N_{Victim} = -C_{VS}N_{Source}. \qquad (1)$$

Here N_{Victim} and N_{Source} are the fluxes in the corresponding pixels of the Victim and Source CCD-amplifiers. ΔN_{Victim} is the flux above background observed in the Victim amplifier. C_{VS} is the fitted coefficient and is different for every CCD-amplifier pair (see link in Appendix A, Table 7 for C_{VS} values). Absolute C_{VS} values measured to be less than 10^{-6} are set to 0. C_{VS} values between amplifiers on the same CCD can be as high as 10^{-3}. All C_{VS} values between CCDs are measured to be less than 2×10^{-4} and most are less than 10^{-5} (Bernstein et al. 2017). These coefficients constitute a Crosstalk Matrix described in Appendix A, Table 6. They were calculated at the beginning of the survey, and have been left unchanged as no significant change has been detected.

The routine that performs the crosstalk correction also runs an overscan correction to remove instrumental bias. Each amplifier has a 50 column wide unilluminated overscan region that spans its entire length. For each row, we compute the mean number of counts across the middle 40 pixels of the overscan region (after removing the minimum and maximum pixel value) and subtract it from the entire row. The overscan mean is calculated independently for each row with no fitting or interpolation between neighboring rows. The use of a row-by-row overscan is particularly important for DECam, because CCDs that share a backplane with the focus CCDs see a bias jump when the focus CCDs finish reading halfway through the science CCD readout. The crosstalk code also splits the full raw exposure into separate single-CCD images, and the single raw Analog-Digital Unit (ADU) plane is converted to a three-layer multi-HDU fits image, consisting of flux, mask and weight layers as HDUs 0, 1 and 2.

3.2. *Generating Calibration Images*

To produce images of sufficient quality for cosmological analysis, we account for a variety of instrumental effects using a series of calibration images. We first perform initial flat fielding of exposures using bias and dome flat corrections. We also correct for CCD nonlinearity and the brighter-fatter effect (Antilogus et al. 2014, Gruen et al. 2015). We produce a Bad Pixel Mask (BPM) to record DECam-specific artifacts as well as sky background templates and star flats to facilitate sky background subtraction from each science image. We remake the above calibration files each time the camera warms up, typically twice per season.

Bias and dome flat images for each filter are taken nightly. In the first year of data taking, these nightly calibration images were used to detrend science exposures during nightly processing. However, it was found that the camera response was more stable than the individual nightly calibration exposures, and after the first year we used a set of "supercals" assembled by combining flats and biases taken over several nights. Our bias images are composed of a mean coadd with 5σ rejection of approximately 150 null exposure time images that have been crosstalk corrected. Similarly, the flat field images are 5σ rejected mean coadds of typically 50-100 short (8s-20s, depending on filter) illuminated dome-flat images that have been crosstalk corrected. A single set of these averaged supercals are adequate for removing the pixel-to-pixel response of the camera for an observing epoch. Nightly calibration images are still used to evaluate camera function.

We also correct for CCD nonlinearity and the so-called "brighter-fatter" effect in all science images and flat images. Estrada et al. (2010) report DECam CCD nonlinearity at both low fluxes and near saturation using flat field images. We correct for this nonlinearity with a CCD-dependent lookup table that converts observed flux to their fitted model of true flux (Bernstein et al. 2017). The brighter-fatter effect is caused by charge building up on well-illuminated pixels and pushing away nearby charge, effectively broadening the PSF of bright objects. Gruen et al. (2015) model this effect for DECam, and we use their CCD-dependent kernel to account for the brighter-fatter effect in the data.

Associated with each observing epoch, we produce a BPM from the flats and biases along with a set of approximately 50 g-band sky exposures. The BPMs are propagated into the mask plane for each CCD image, which also includes "bad pixel" information specific to each exposure. The BPM bit mask is provided in Appendix A, Table 8. Pixels with values less than 50% the mean (over the full camera) in any of the inputs to the flat coadd image are flagged as being cold (FLAT_MIN). Similarly, pixels with values greater than 150% of the mean in three or more input images are marked as hot (FLAT_MAX). Pixels with more than 500 photo-electrons in any of the input bias images are flagged as hot (BIAS_HOT) while those with more than 20 photo-electrons are flagged as warm (BIAS_WARM). Pixels within a 11×3 rectangle (along the readout direction) centered at a hot pixel are also marked as warm. Columns with multiple hot pixels are marked as BIAS_COL. All pixels read out after a hot pixel are also marked as BIAS_COL. Pixels read off $60 \times N$ (60, 120, 180 ...) pixels before a hot pixel are problematic and are also marked as BIAS_COL.

The BPM images include static masks that capture persistent systematic issues with DECam. Pixels within the 15 rows or columns nearest the edge are unsuitable for quantitative measurement and marked as EDGE. We have observed several regions in the flats with persistent structure in the readout direction, including persistent defects and smearing. Rectangles around these regions have been manually marked. In addition, each hot pixel has a small region around it where the brighter-fatter correction will produce anomalous results. Neither of these effects is modeled quantitatively, although both appear to be quite small. Pixels affected by these effects are marked as SUSPECT for exclusion from particularly precise tasks. Similarly, some columns have significantly different sky levels than their neighbors but no obvious difference in the bias and flat images and are manually marked as FUNKY_COL. Regions with an inconsistent response detected in stacks of sky exposures are marked as WACKY_PIX. We do not use amplifier A of DECam CCD 31, because its gain is unstable at the 10% level, and it is marked BADAMP. The star flat correction is unreliable on the 1-2% level within 25 columns of either CCD edge and the data here is marked NEAREDGE. Finally, each CCD contains six roughly 1.5 mm "tape bumps" where two-sided tape was placed to maintain the relative position of and spacing between the CCD and its aluminum nitride readout board (Derylo et al. 2006). These tape bumps have unstable electrostatic properties (compared to other locations on each sensor) that affect both photometry and astrometry in ways that change with each thermal cycle of the camera. These regions are marked TAPEBUMP and, similar to SUSPECT regions, may not be usable for some applications. Overall, typically 3% of pixels are flagged as being on or near the edge of the CCD, and an additional 0.2% of pixels have some other flag that makes them unusable (excluding the unusable half of CCD 31). Roughly 1% of pixels are marked TAPEBUMP or SUSPECT.

We need a sky background model to subtract from our images (Section 4.3). We use a set of 1000 exposures from a given epoch to create an outlier-subtracted sky model defined in terms of four Principal Component Analysis (PCA; Jolliffe 1986) components. The first component is a median image that includes the pupil effect (a scattered light torus) on large scales and fringing which is strongest in the z and Y bands on smaller scales. These two effects were handled with a separate routine in earlier instances of the processing pipeline (Drlica-Wagner et al. 2017). The second and third components are smooth, orthogonal gradients. The fourth component contains the pupil and fringe patterns in a different ratio from the first component and allows us to account for variations in the ratio of airglow to moonlight. Higher order components do not appear to be physically meaningful. The PCA components are represented both as full-resolution images over the exposure plane and as lower resolution maps consisting of the median of each 128×128 block of pixels (called a "superpixel"). Individual exposures can be robustly fit with the low resolution images, and the corresponding full resolution background can be subtracted off. Bernstein et al. (2017) describes the background model in more detail.

We derive a "star flat" that quantifies the differences between the dome flat and the true response to astronomical flux. These are composed of 22 exposures of 30 seconds each taken in different moderate density star fields. We dither these exposures by angles ranging between $10''$ and 1 degree so that the same star will fall on many different locations across the focal plane. We then process these images identically to science exposures up to this stage and make stellar catalogs using SEXTRACTOR (Bertin & Arnouts 1996). We can then use these stars to model the spatial and color variation of response of the camera and optical system. Bernstein et al. (2017) describes these star flats in more detail.

3.3. *Flat Field Correction and Initial Masking*

Having produced a series of image calibration files (see Section 3.2), we can perform flat field correction and initial pixel masking. We use the DES-specific tool, PIXCORRECT[4], to apply our image calibration operations to the crosstalk-corrected images in the following order:

1. Subtract a bias image

2. Apply a nonlinearity correction

3. Mask saturated pixels

4. Apply a bit mask to the science image

5. Correct bit mask columns where appropriate

6. Apply a gain corrections

7. Apply a brighter fatter correction

8. Divide by the dome flat

These steps are applied separately to each CCD image of each DECam exposure. Each CCD image consists of a three-layer FITS file including flux, mask, and weight HDUs. The mask layer is initialized to the BPM for that CCD. Later processing steps set bits in the mask layer for bright star bleed trails, edge bleeds (see below), detected cosmic rays, and detected satellite streaks (the flux layer is modified in special cases where known bad pixels can be fixed, and to correct effects such as non-linearity, crosstalk and brighter-fatter). The weight plane layer is initially set to the inverse variance weight calculated from the sum of the variance in the number of photoelectrons in each pixel and the variance of the readout noise.[5] This weight is used in initial masking and to fit the sky background. After fitting the sky background, the weight layer of each image is replaced by the best-fit sky model in photoelectrons (Section 4.3).

Our bias subtraction is a simple pixel-by pixel subtraction of the (crosstalk-corrected) bias image. We perform the nonlinearity correction for each pixel using the precomputed CCD-dependent lookup table described in Section 3.2. We mask those pixels whose values exceed their saturation values with the SATURATE bit in our bitmask (described below). Saturation values are different for each amplifier and are noted in the image headers. Typical values are $\sim$175,000 photo-electrons ($\sim$44,000 ADU).

We use the BPM images from Section 3.2 to produce an initial bitmask for the image. All of our bitmask codes are defined in Appendix A, Table 9 (prefaced with BADPIX), but we only set some of the bits at this processing stage. The remaining mask bits are set by the saturation and bleed masking routine (Section 4.2) and the cosmic ray and streak masking routine (Section 4.4).

We initially mark all image bits with a corresponding BPM bit of FLAT_MIN, FLAT_MAX, BIAS_HOT, BIAS_WARM, BIAS_COL, FUNKY_COL or WACKY_PIX as BPM. Columns marked with BPM bit of FUNKY_COL and partial columns marked as BIAS_COL (those pixels read out before a hot pixel in their column) can often be corrected by subtracting a constant offset as follows. If half of the nearest twelve

columns (six in either direction) to a FUNKY or partial BIAS column are normal, we calculate an outlier clipped mean and variance (with an additional linear slope subtracted from the column) for each column. We take the average of these values across all comparison columns to produce a "comparison mean" and a "comparison variance." If the BIAS or FUNKY column's variance is within 25% of the comparison variance, we subtract off the difference between the column's mean and the comparison mean so that the column has the same mean value as its comparison mean. The FUNKY or partial BIAS is then relabeled as FIXED in the image mask. The corresponding BPM bits are then unset. Columns without six acceptable neighboring columns (among the twelve columns described above) or columns whose variance is more than 25% greater than their comparison variance remain marked as BPM.

The BPM bits of EDGE, SUSPECT, NEAREDGE and TAPEBUMP are passed directly into the image mask with the corresponding bitmask bit. The actual values of these flags are different in the BPM and image mask (see Tables 8 and 9).

Our final three steps are simple operations. We use our (amplifier-specific) gain correction to convert from ADU to electrons. This correction is roughly a factor of 4 for DECam. We apply the brighter-fatter correction (Section 3.2). We finally apply the flat field correction, dividing the image by the dome flat values. Mathematically, the calibrated pixel value, CAL, is:

$$\mathrm{CAL} = \frac{\mathrm{BF}(\mathrm{Lin}(\mathrm{RAW} - \mathrm{BIAS}) \times \mathrm{GAIN})}{\mathrm{FLAT}}, \qquad (2)$$

where Lin is our linearization correction, GAIN is a multiplicative gain constant, BF is our brighter-fatter correction and RAW, BIAS and FLAT are (crosstalk-corrected) raw, bias and dome flats, respectively. GAIN is an amplifier-specific conversion between the ADU and the more physical unit of photo-electrons.

At this point, we have also made an inverse variance weight image to go along with the science image. This weight image includes noise from the bias and flat images added in weighted quadrature to the initial image Poisson noise. Pixels marked with EDGE and BADAMP are given zero weight value.

For the first two years of the survey, images were processed slightly differently. Particularly, saturation masking was performed as part of the crosstalk correction, and the brighter-fatter correction was not performed at all. All processed data in the public data release, including the reprocessed Y1 and Y2 data, were processed with the above methods.

4. FIRST CUT AND FINAL CUT

We use the First Cut pipeline to process all DES exposures within a few hours of acquisition so that they can be evaluated for depth and image quality. Exposures that do not meet our survey quality criteria are flagged as such, and that area is reobserved on a subsequent night. Rather than settling on a static evaluation pipeline, we have elected to periodically update the First Cut pipeline to incorporate improvements as the survey progresses. This strategy was crucial for the evolution of the supernova difference imaging pipeline and has allowed the DES Collaboration to perform initial investigations using the best reduction of the survey data in real time. In practice, the First Cut pipeline in use at any time during the survey is similar to the Final Cut (Section 4.8) used in the latest release production campaign. One crucial difference is that First Cut processing uses preliminary image calibrations (Section 3),

---

[4] https://github.com/DarkEnergySurvey/pixcorrect
[5] The number of photoelectrons per pixel is calculated from the ADU per pixel by dividing by the gain of each CCD amplifier

necessarily composed of data taken before the science exposure, while Final Cut uses final image calibrations that make use of the entire season.

The basic outline of the First Cut pipeline is:

1. Calculate initial astrometry solution (Section 4.1)

2. Mask saturated pixels and associated bleed trails (Section 4.2)

3. Fit and subtract sky background (Section 4.3)

4. Divide out star flat (Section 4.3)

5. Mask cosmic rays and satellites (Section 4.4)

6. Model the point spread function (Section 4.5)

7. Produce single epoch catalogs (Section 4.6)

8. Evaluate image data quality (Section 4.7)

We describe these steps in detail and point out major changes between the initial First Cut used during SV and Y1 and more modern versions in the remainder of this section. Section 4.8 describes the small differences between our First Cut and Final Cut processing. The latter is used to produce consistently processed data for our cosmological analyses and public data releases.

4.1. *Initial Astrometry*

We compute a single-exposure astrometric solution using SCAMP (Bertin 2006) which is part of the Astro-Matic suite of astronomy software.[6] We generate SEx-tractor(Bertin & Arnouts 1996) catalogs of bright objects that are read by SCAMP and matched the bright sources in archival reference catalogs with reliable astrometry. We use this initial astrometric solution to match our stars to reference catalogs for initial photometric calibration and PSF modeling. We later improve this solution with multiple DES exposures for our final analysis (Section 6.2).

The astrometry input catalogs were generated by SEx-tractor using the settings described in Appendix B, Table 10. These catalogs were generated with a higher detection threshold and less deblending than typical science catalogs (e.g., in Section 4.6) to minimize spurious detections. It also assumes an initial seeing FWHM of $1''2$ since the PSF has not yet been modeled. SEXTRACTOR requires contiguous pixels to be above a detection threshold, and its performance is generally improved if one convolves the image with a small kernel to remove noise that dominates at scales smaller than the PSF. To avoid compromising deblending, we convolve our image with a standard 3×3 pixel "all-ground" filter (values 4 in the middle, 1 in the corners and 2 on the sides). We use the same filter for all other SEXTRACTOR uses except for difference image object detection in Section 5.4 and the final coadd catalog in Section 6.5. This convolution is internal to SEXTRACTOR, and the image is unchanged for later analysis.

We match these sources across the entire exposure with SCAMP to a reference catalog using the settings in Appendix B, Table 11. SCAMP calculates an astrometric solution with a TPV World Coordinate System (WCS; Calabretta & Greisen 2002). It takes as input a fixed initial-guess set (calculated

from a set of earlier exposures) of PV third order WCS distortion terms for each of the 62 CCDs in the DECam array. SCAMP also calculates the typical astrometric error between our stars and those in the archival reference catalog. In our initial implementation we used the UCAC4 stellar catalog (Zacharias et al. 2013) as our reference catalog. In Y4, we found that using the 2MASS point source catalog (Skrutskie et al. 2006), which has higher source density than UCAC, prevents rare SCAMP failures, and we began using it instead. We have typical DES-2MASS difference of $0''25$. These errors are dominated by 2MASS which has typical single detection uncertainties of $0''2$ for sources fainter than K_S of 14 which we match to. In addition, the proper motion of stars between the 2MASS epoch and DES epoch is not corrected for and contribute to these differences. Section 6.2 shows how we ultimately achieve a relative, internal DES uncertainty of $\approx 0''03$ by combing overlapping exposures. Future processing of DES data with the Gaia catalog (Gaia Collaboration 2016) as a reference will allow DES to reduce relative and absolute astrometry uncertainties to below $0''03$.

4.2. *Saturation and Bleed Trail Masking*

In addition to the masking of pixel artifacts described in Section 3.3, we also mask saturated pixels, streaks and cosmic rays. Here we discuss the masking of bright stars, their associated charge overflow in the readout direction (called "bleed trails"), and the build up of charge they cause near the edge of CCDs. Pixels with any of these effects are generally not usable. We describe our procedure for masking satellite streaks and cosmic rays in Section 4.4. The flags mentioned here are listed in Appendix A, Table 9.

Many image-specific artifacts are from bright stars and their associated bleed trails. We initially identify bleed trails as saturated columns along the readout axis of the image. They are caused by charge spreading along the readout columns from a saturated object. Our algorithm searches for trails with a 20×1 pixel kernel (long in the readout direction) and requires 7 contiguous saturated pixels to trigger. It then finds all saturated pixels adjacent to this kernel to identify an initial trail. This trail is typically hundreds of pixels long and includes the bright star. We extend this region by 6 pixels orthogonally to the readout direction to compute a rough estimate of the area that will be masked. We then produce a rectangle 5 times bigger than this region in both the x and y direction. We fit the background in non saturated area of this rectangular region, iteratively rejecting 5σ outliers (using up to 100 iterations). All pixels in a contiguous region from the saturated trail down to where the flux goes below 1σ above the fitted background are masked as TRAIL.

We have not yet differentiated the actual saturated star from its corresponding bleed trail. Using a stellar center defined by the median bin in our initial saturated trail, we fit a circle with a radius such that its outermost pixels have a value that is 3σ above the background (as calculated in the previous paragraph). We mask all pixels within 2 times this radius as STAR. If the bleed trail reaches the read registers, we search for deviations in the background light near the CCD edge of the amplifier containing the bleed trail. The pixels in a rectangular region where the background deviates by more than 1σ are flagged as EDGEBLEED (see Fig. 5 of Bernstein et al. 2017).

Finally, we mask the pixels at the analogous position of a bleed trail in the neighboring amplifier on the same CCD as SSXTALK, because the crosstalk signal from saturated pix-

els is not properly corrected by our linear crosstalk algorithm (Section 3.1).

4.3. *Sky Subtraction*

To isolate astronomical sources and remaining artifacts from the field, we must first subtract a background component from the image. To do this, we fit and subtract off a sky background image using the PCA templates from Section 3.2 and divide our image by a nightly star flat.

We describe the production of sky template images in Section 3.2. We bin our science images into the same low resolution superpixels as the templates (the median of 128×128 pixel square). We then fit this low resolution image with the 4 corresponding low resolution PCA templates. We multiply our 4 full resolution PCA sky template images by these 4 PCA coefficients to produce a full-resolution sky background model. We subtract this image from the science image. At this stage, we produce an updated weight image from the inverse variance of the number of photo-electrons in the sky model. This avoids a statistical bias in weight in which pixels with positive fluctuations are are given more weight than those with negative fluctuations.

This algorithm for fitting and removing sky for Y3A2 works on the whole DECam exposure at once, rather than normalizing on a CCD-by-CCD basis as was done in Y1A1. This results in important improvements to the overall sky fitting and background removal. This is particularly important for detecting extended objects that cover areas more than 1 arcminute in extent (i.e. extended light from galaxy clusters or very faint extended low surface brightness objects). We refer the reader to Bernstein et al. (2017) for a full description of the sky subtraction algorithm.

At this point, the image is divided by the star flat (Section 3.2) to correct the differences between the dome flat and the true response to stellar flux. Following division by the star flat, First Cut and Final Cut image processing is nearly complete. Fig. 6 shows a sample exposure with all the above processing steps applied. This is DECam exposure number 164189, a 100 second *r*-band image of the Omega Centauri globular cluster field.

4.4. *Cosmic Ray and Satellite Masking*

Having subtracted the background image and performed the masking associated with the bad pixels in Section 3.3 and saturated pixels in Section 4.2, we now mask our final artifacts: cosmic rays and streaks. Masking cosmic rays and streaks in DES was investigated in Desai et al. (2016); however, those algorithms are not applied in First Cut or Final Cut processing.

When cosmic rays interact with the silicon of the DECam CCDs they produce image artifacts that can range in appearance from small dots to long streaks. These defects are distinct because they affect a few adjacent pixels and are not convolved with the PSF. To detect cosmic rays, we use a variant of the cosmic ray detection algorithm from the LSST code base (Jurić et al. 2015). This algorithm examines all pairs of opposing pixels (i.e. the north-south pair, the east-west pair, the NW-SE pair and the NE-SW pair) surrounding each pixel. We define a cosmic-ray pixel to be 6σ above the mean of each of the four pairs (where σ is calculated from the local sky background). We also require:

$$I_{pix} - 1.5\sigma_{pix} > 0.6 P_{pair}(I_{pair} + 1.5\sigma_{pair}) \qquad (3)$$
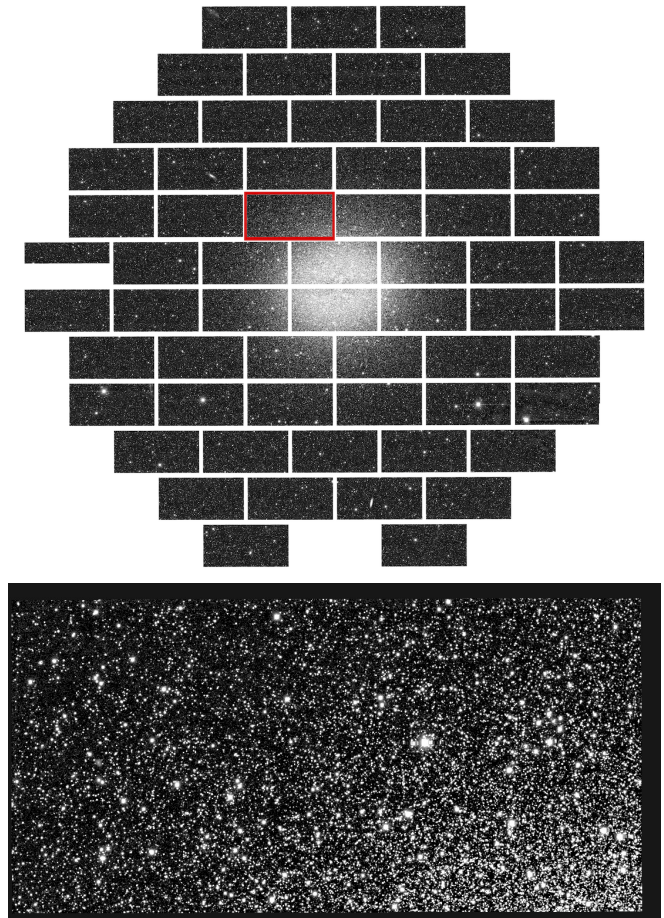
Figure 6. DECam exposure number 164189, a 100 second *r*-band image of Omega Centauri. The top panel shows the full camera image. CCD 2 is functional in this image, and contains data. CCD 61 and the lower half of CCD 31 are unusable and blacked out. The bottom panel shows a zoom in of CCD 22, which is boxed in red in the top panel.

for at least one pixel pair. Here, I_{pix} and σ_{pix} are the intensity and background uncertainty of the pixel in question while I_{pair} and σ_{pair} are the mean intensity and uncertainty of the mean for one of the four pairs. P_{pair} is the expected average value of the PSF for each pair (with the PSF normalized to unity at the central pixel). This second requirement indicates that background gradient is not changing faster than the PSF for at least one neighbor pair and takes advantage of the fact that at least one neighbor pair will generally be unaffected by the cosmic ray. Pixels that satisfy this requirement as well as their neighbors (including diagonal neighbors) are masked with the BADPIX_CRAY bit.

Streaks are caused by satellites crossing the field of view or linear image defects, and they appear as elongated luminous regions often several arcseconds wide and many arcminutes long. The Hough Transform (Duda & Hart 1972) extracts features (typically lines) from an image. To perform our Hough transform, we ignore all previously masked pixels and dilate our masks around bleed trail masks (Section 4.2). This includes diagonal dilation. We then bin the image into 8×8 superpixels, mark superpixels more than 1.5σ above the mode and perform a Hough transform on the binary mask image of marked and unmarked pixels. We detect peaks in the Hough transform image as 18σ overdensities. The contiguous area around the Hough peak that exceeds 12σ is marked as a Hough peak. The Cartesian coordinates of this point in

Hough space are related to the angle, θ, that a line makes with the image and the line's distance from the center of the image. Peaks that cover a θ range of more than $75°$ in Hough space or peaks that are more than 300 pixels wide are ignored to avoid excessive masking. Finally, we ignore Hough peaks that have less than 33% of their pixels exceeding the 1.5σ threshold. Real pixels corresponding to the remaining Hough peaks are masked with the `BADPIX_STREAK` bit.

At this stage, we also assign 0 weight to pixels with the `BADPIX` mask bit `BADAMP`, `EDGEBLEED` or `EDGE` or `CRAY` set. Before Y3 processing, masked cosmic ray regions were interpolated across during this masking. But after Y3 (including all Y1 and Y2 data reprocessed for public release), this feature was removed as these regions have zero weight.

4.5. *PSF Extraction*

We model the point spread function (PSF) of each image individually using PSFEx (Bertin 2011), a PSF analysis package part of the ASTROMATIC suite of astronomy software. The first step in using PSFEX is to make a "bright star" catalog for each CCD image using SEXTRACTOR and the parameters in Appendix B, Table 12. Parameter values differ slightly from those used in Y1. We convolve the image with the same 3×3 pixel "all-ground" convolution mask from Section 4.1.

We use these bright star catalogs and their accompanying images as inputs for PSFEx using the parameters in Appendix B, Table 13. PSFEx takes unsaturated point sources from the catalogs, examines each object and iteratively models the PSF while excluding non-PSF sources. Ultimately, PSFEx produces a model of the PSF across each CCD of every on-sky exposure. For Y3, the model varies with degree 2 (quadratically) across each 4096×2048 CCD. The PSF modeling described here is used for the photometry in our official data release. Some DES analyses (e.g. weak lensing described in Zuntz et al. 2017) use different PSF modeling.

4.6. *Single Epoch Catalog Production*

We use SEXTRACTOR to produce source catalogs for individual images. The parameters we use are described in Appendix B, Table 14 and we convolve the data with same 3×3 pixel "all-ground" filter from Section 4.1. We use the fitted PSF models described in Section 4.5. The measured parameters include those described in Table 3. The detection threshold for the Final Cut catalogs corresponds to $S/N \sim 10$. We note that the output catalogs include the parameter `IMAFLAGS_ISO`, which expresses the union of all mask bits present for pixels within the isophotal radius of each source.

4.7. *Image Evaluation*

DES used historical observing conditions at CTIO to establish a series of survey requirements which translate into requirements on the PSF, background and atmospheric transmission that each exposure must satisfy to be included in the final wide-area survey. We combine these three quantities into a value called $t_{\rm eff}$, which we use to evaluate image quality (Neilsen et al. 2015). We also impose separate requirements on the PSF and sky background.

$t_{\rm eff}$ is the ratio between the actual exposure time and the exposure time necessary to achieve the same signal-to-noise for point sources observed in nominal conditions. An exposure taken under "fiducial" conditions has $t_{\rm eff} \equiv 1$. These fiducial conditions (Table 4), are above average, but not uncommon

Parameter	Description
`ALPHAWIN_J2000`	Right ascension
`DELTAWIN_J2000`	Declination
`FLAGS`	Detections flags
`FLUX_AUTO`	Kron flux
`FLUXERR_AUTO`	Kron flux uncertainty
`FLUX_PSF`	PSF flux
`FLUXERR_PSF`	PSF flux uncertainty
`A_IMAGE`	Major elliptical axis
`B_IMAGE`	Minor elliptical axis
`THETA_IMAGE`	Elliptical position angle
`IMAFLAGS_ISO`	Isophotal image flags
`SPREAD_MODEL`	Non-PSF flux parameter
`SPREADERR_MODEL`	Non-PSF flux error

Table 3
Output SEXTRACTOR quantities reported in single epoch catalogs.

Filter	$FWHM_{fid}$ (arcseconds)	B_{fid} (electron s^{-1})	Minimum $t_{\rm eff}$	$FWHM_{max}$ (arcseconds)
g	0.9927	1.05	0.2	1.765
r	0.9369	2.66	0.3	1.666
i	0.9	7.87	0.3	1.6
z	0.8685	16.51	0.3	1.544
Y	0.8550	14.56	0.2	1.520

Table 4
The fiducial and limiting values for parameters used in our First Cut image evaluation.

for CTIO. Specifically, we define

$$t_{\rm eff} \equiv \left(\frac{FWHM_{fid}}{FHWM} \right)^2 \left(\frac{B_{fid}}{B} \right) F_{trans}. \qquad (4)$$

$FWHM$ and $FWHM_{fid}$ are the measured and fiducial PSF full width half max, respectively. B and B_{fid} are the measured and fiducial sky background. F_{trans} is the atmospheric transmission relative to a nearly clear night.

$FWHM_{fid}$ are listed in Table 4. To obtain these values, we multiply a $FWHM$ of $0.''9$ in the i band by a coefficient calculated with a Kolmogorov turbulence model (Roddier (1981), Kolmogorov (1941)) that converts between i-band seeing and the seeing that would be observed in another band. We have calculated a set of DECam sky brightnesses from a "photometric" night (2012 December 15) to obtain our fiducial B, listed in Table 4.

We calculate atmospheric transmission as a robust, outlier-rejected median difference between the First Cut stellar magnitudes and those from well-calibrated datasets. We compare DES i, z and Y magnitudes to 2MASS point source J magnitudes (Skrutskie et al. 2006) accessed via the Naval Observatory Merged Astrometric Dataset (NOMAD; Zacharias et al. 2004). We compare the DES g- and r-band magnitudes to their counterparts in the The AAVSO Photometric All-Sky Survey (APASS; Henden et al. 2009) when these catalogs are deep enough and a combination of NOMAD J and B band (Monet et al. 2003) otherwise. We convert this magnitude difference, Δm, to a multiplicative transmission factor:

$$F_{trans} = 1, \text{ for } \Delta m \leq 0.2,$$
$$F_{trans} = 10^{-0.8(\Delta m - 0.2)}, \text{ for } \Delta m > 0.2. \qquad (5)$$

We reject exposures with $t_{\rm eff}$ less than the minimum values listed in Table 4. In practice, this is usually the most stringent image requirement. We also require i-band seeing to be less

than $FWHM_{max}$ (Table 4). $FWHM_{max}$ was constructed using the same Kolmogorov conversions as $FWHM_{fid}$ and the constraint that the i-band PSF have $FWHM < 1\rlap{.}''6$.

OBSTAC uses onsite monitors to estimate sky brightness and seeing before an image is taken. If OBSTAC estimates that the i-band seeing at zenith does not satisfy $FWHM_i < 1\rlap{.}''1$, it schedules observations of supernova fields that have not been observed in four or more nights. If OBSTAC estimates that the sky background may exceed acceptable limits, it does not schedule observations in g or r band, and, in extreme cases, it restricts observations to the Y band.

4.8. *Final Cut*

As mentioned above, we process each wide-area exposure at least twice: First Cut processing is run within a few hours of acquisition and Final Cut processing is run months later to assemble a data release with an improved version of the software.

In addition to the relatively minor code changes between the First Cut and the Final Cut pipelines, we also used different calibration images. Specifically, during the first three years of First Cut processing, we calibrated the images using nightly calibration images. All Final Cut processing as well as our First Cut processing after Y3 use super-calibration images (Section 3.2) with larger number of input images for more statistical power. The processing of calibration images themselves is also updated analogously to the processing of their corresponding science exposures.

Final Cut data is photometrically calibrated using Forward Global Calibration Method (FGCM; Burke et al. 2018). This method uses overlapping exposures and a large network of calibration stars to calibrate the entire survey while also modeling the time-dependent atmospheric and instrumental passbands for each CCD. FGCM assigns each exposure a zero point with typical uncertainty of 7 mmag.

There will be at least three DES data releases internal to the DES Collaboration (Y1, Y3 and eventually Y5). Each release includes all the data up to that point. The DR1 public release includes all data through Y3, and the DR2 public release will include all data up to Y5 (all DES data). For each release, every exposure taken at that time is processed with the current Final Cut pipeline. There were significant software changes between the beginning of the survey (SV, Y1) and the Y3 data release, the first data release with complete coverage of the survey footprint. We anticipate additional incremental improvements through Y5. As the processing software asymptotically approaches its final form, the First Cut and Final Cut pipelines merge, with the Y5 First Cut being essentially identical to Y4 Final Cut.

5. SUPERNOVA PROCESSING

Detecting and characterizing Type Ia supernovae is one of the primary goals of DES. The wide-area cadence includes two observations of each area per band per season, which is not adequate for transient light curve characterization. Instead, DES repeatedly visits ten 3 deg^2 fields when OBSTAC estimates that observation conditions are marginal (PSF FWHM worse than $1\rlap{.}''1$ when transformed to i-band zenith) or when any supernova field has not been observed in seven nights. Roughly 45% of supernova data is taken in conditions that fail the First Cut quality requirements described in Section 4.7.

To cover a range of supernova luminosities and implied redshifts, we observe 8 "shallow" fields (C1, C2, E1, E2, S1, S2,

| Field	Deep or Shallow	Field Center (deg) R.A.	Decl.
C1	shallow	54.2743	-27.1116
C2	shallow	54.2743	-29.0884
C3	deep	52.6484	-28.1000
E1	shallow	7.8744	-43.0096
E2	shallow	9.5000	-43.9980
S1	shallow	42.8200	0.0000
S2	shallow	41.1944	-0.9884
X1	shallow	34.4757	-4.9295
X2	shallow	35.6645	-6.4121
X3	deep	36.4500	-4.6000

Table 5
The location of each supernova field in right ascension and declination.

X1 and X2) and 2 "deep" fields (C3 and X3). Table 5 shows the center of each field. These fields were chosen to avoid bright stars and to overlap with other significant surveys. The C fields overlap with the Chandra Deep Field South (Xue et al. 2011). The E fields overlap with the ELAIS S1 field (Gruppioni et al. 1999). The S fields overlap with SDSS stripe 82 (Adelman-McCarthy et al. 2007, Abazajian et al. 2009). The X fields overlap with the XMM-LSS fields (Pierre et al. 2004). The exposure times of each field in each band are in Table 1. The shallow-field g, r and i observations in a given night are single exposures. The shallow z observation and all deep observations are coadditions of exposures taken in uninterrupted sequences. Going forward, we refer to an individual night's observation as an "epoch" regardless of the number of exposures taken.

We process the supernova fields with essentially the same pipeline as the wide-area First Cut pipeline up through the second masking phase (Section 4.4). After an image has been processed, we refine its astrometric solution and match it to a template image of the same field. We then subtract the template image from the nightly science image, detect sources in the resulting difference image, cross-correlate difference detections across different images and evaluate our transient detection efficiency by analyzing artificially inserted sources in the images. We diagram this pipeline in Fig. 7 and summarize it in this section. Kessler et al. (2015) describes the DES supernova program and algorithms in more detail. Here we give an operational description on how our software is run and how the supernova processing fits into the context of DES processing.

5.1. *Supernova Calibration*

Supernova characterization for spectroscopic follow-up requires more precise photometric calibration than the typical First Cut wide-area processing. We facilitate the First Cut photometric calibration by imaging standard star fields during both evening and morning twilight (Tucker et al. 2007). These standard star fields are generally in SDSS Stripe 82 or at declination $\approx -45°$ (Appendix A of Drlica-Wagner et al. 2017). We use stars from these fields (called secondary standard stars) to determine nightly zero points, atmospheric extinction coefficients and color terms. We then use a set of "tertiary standard stars" within each of the supernova fields for photometric calibration. The fields and the tertiary standards within them were observed in photometric conditions during the Science Verification period, and their magnitudes and colors are well-measured relative to the nightly standards. In good conditions, we typically have 100–200 tertiary standards per CCD in each field. Relative and absolute photo-
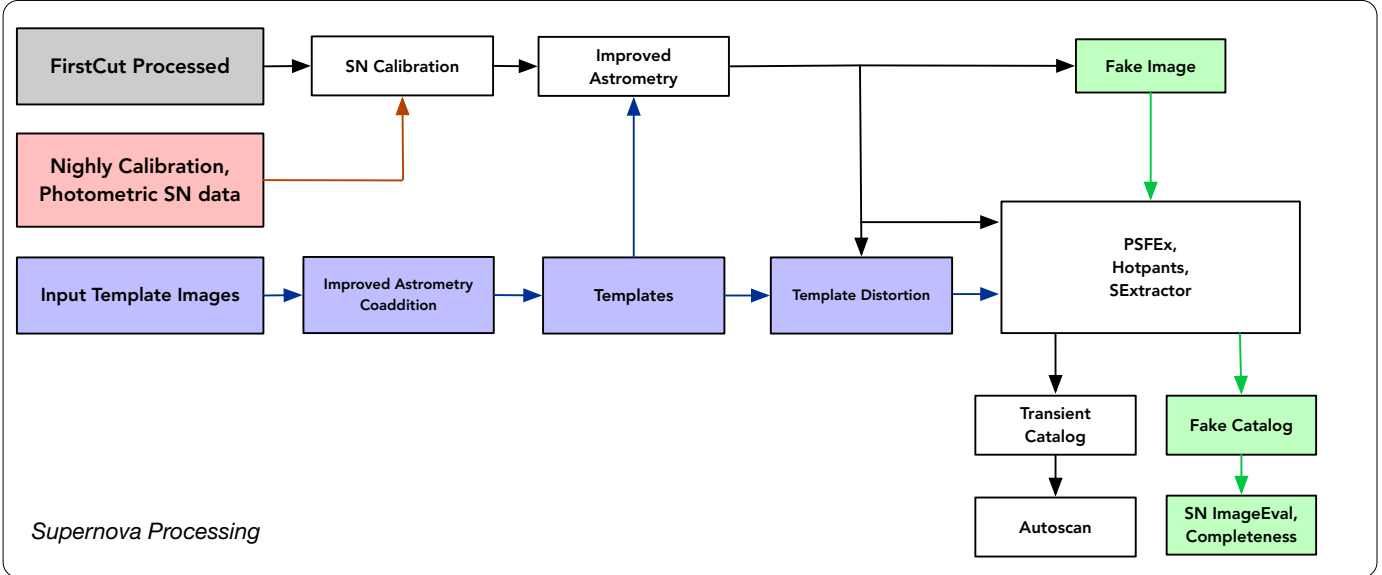
Figure 7. A diagram of the difference image processing used to detect supernovae and other transient in the DES supernova fields.

metric calibration have been confirmed to the 2% level in the difference imaging pipeline (Kessler et al. 2015), and calibration continues to improve for the cosmology analysis (Burke et al. 2018).

5.2. *Supernova Template Images and Improved Astrometry*

Our supernova detection algorithm depends on precise image subtraction between a nightly science image and its corresponding template image. This "difference imaging" requires template images that are astrometrically aligned to the science image.

We produce a coadded template image per season for each field from exposures from a different season. The Y1 templates were constructed from science verification data for the initial detection and then remade with Y2 data for later reprocessing. The Y2 templates were made with Y1 data, and all later templates were made from Y2 data. For each CCD of each template, we find the image with the lowest sky noise, σ_{SKY}^{min}, and then make a coadded image from the epochs with the sharpest PSF that have sky noise less than $2.5\sigma_{SKY}^{min}$. The coadd can include up to 10 epochs, though the average contains 8.4 that satisfy the noise requirement.

We find our template image astrometric solution in two steps. First, each exposure in the template is aligned with SCAMP (Section 4.1) to the the USNO-B1 catalog (Monet et al. 2003) with precision of roughly 100 mas. We calibrate the images (see Section 5.1) and make a weighted intermediate coadd of these exposures. We use the resulting catalogs of stars to make a new reference catalog of relative astrometric standards. We re-align the constituent exposures to this coadd catalog, resulting in 20 mas (0.08 pixel) relative precision. In the nightly supernova image processing, we use the same coadd reference catalog to improve the astrometric solution, typically achieving relative astrometric precision between the single epoch image and template of roughly 25 mas (0.1 pixel). In addition to using an improved reference catalog, the supernova pipeline (which was developed independently of the First Cut pipeline) uses different astrometry catalog SEXTRACTOR settings (Appendix C, Table 15) and

SCAMP settings (Appendix C, Table 16).

5.3. *Supernova PSF Modeling*

The PSF modeling in the supernova pipeline uses PSFEX but was developed independently of the analogous routines in the wide-area pipeline. We use SEXTRACTOR and the settings in Appendix C, Table 17 to make a catalog of sources for PSFEX analysis. We also use the "all-ground" filter from Section 4.5. In addition, we match the sources detected here to a previously defined list of pointlike objects constructed from high quality Science Verification data in the supernova fields. We then model the PSF with PSFEX and the settings in Appendix C, Table 18.

5.4. *Detecting Transients in Difference Images*

We detect transients as point sources in the difference images. To produce these images, we astrometrically distort the template images to match the corresponding single epoch image, model and match the PSFs in the science and template images and finally detect sources in their difference.

We astrometrically resample the template images using SWARP (Bertin et al. 2002), part of the ASTROMATIC software package. Using the astrometry headers created by SCAMP (Section 4.1), and settings in Appendix C, Table 19, SWARP matches the template image to the science image from each epoch on a pixel by pixel level. Alignment is typically accurate to roughly 0.1 pixels. At this point, we also use SWARP to produce nightly supernova coadd images (shallow field z-band images and all deep field images). The SWARP settings for coaddition are nearly identical to those in Table 19 except that RESAMPLING_TYPE = LANCZOS3 and PROJECTION_ERR = 0.001.

We photometrically match the (astrometrically-matched) template image to the science image using HOTPANTS (Becker 2015) and the parameters in Appendix C, Table 20. Briefly, HOTPANTS divides a CCD image into 200 (10×20) stamps. Within each stamp it detects stars and estimates the optimal kernel needed to convolve the template image of the star into the science image. HOTPANTS then uses these

measurements to model a spatially varying kernel across the entire image which it in turn uses to produce a convolved template image. This kernel includes a spatially-varying scaling term to match the images photometrically. The convolved template and the science image are now ideally matched in astrometry, photometry and PSF. HOTPANTS outputs a kernel model and difference image which should ideally be consistent with zero excluding transients.

We find the point sources for the difference image using SEXTRACTOR and the parameters in Appendix C, Table 21. SEXTRACTOR filters (convolves) the difference image using a 5×5 pixel Gaussian with a FWHM of 3 pixels. The resulting catalog of transient detections contains significant contamination and requires automatic artifact rejection (Section 5.6).

5.5. *Fake Images*

To assess our transient detection efficiency we add simulated transients, "fakes," to each supernova exposure. The transients are inserted as point sources (as modeled by PS-FEx). There are ≈ 20 fakes per CCD. Only a negligible fraction of galaxies have a fake in any given image, and fakes have a correspondingly small impact on transient completeness.

We add two classes of fake sources to the images: isolated 20th magnitude sources and sources that simulate a set of Type Ia supernova that span the full range of redshifts and supernova-host separations (as per SNANA; Kessler et al. 2009, 2015). We use the 20th magnitude fakes to evaluate image depth and determine if an image needs to be retaken (Section 5.7). We use the Type Ia supernova fakes to measure detection efficiency versus signal-to-noise (needed for simulations), and to monitor the trigger efficiency versus redshift.

5.6. *Transient Candidate Evaluation*

Difference images are prone to unique artifacts, and we use more stringent criteria than in conventional astronomical images to ensure that the difference image point sources are real. Difference image point sources must satisfy a series of pixel and catalog-based requirements. We make postage stamps of sources that pass these cuts and pass these on to a more rigorous selection routine called AUTOSCAN, described below.

To eliminate the bulk of artifacts, we apply basic quality cuts. Potential transient candidates must be brighter than 30th magnitude, have signal to noise greater than 3.5 (typically less stringent than the 5σ SEXTRACTOR requirement) and be consistent with a point source PSF (as measured by the SEXTRACTOR parameter SPREAD_MODEL). In a 35×35 pixel stamp around the candidate, there must be fewer than 200 pixels 2σ below the mean, 20 pixels 4σ below the mean and 2 pixels 6σ below the mean. This helps reject "dipoles" (negative regions abutting positive regions), a common form of artifact in difference images caused by astrometric misalignment. We also reject objects coincident with known photometric variables (including quasars) and bright stars from a previously-defined veto catalog. We enter all sources that pass these cuts into a database that includes the transient detection from previous images.

Difference sources that pass the above criteria are saved as 51×51 pixel stamps and sent to AUTOSCAN, a more rigorous selection algorithm described in Goldstein et al. (2015). AUTOSCAN is a machine learning selection algorithm that was trained with a set of 900,000 transient detections. Half are synthetic transients (the Supernova Ia "fakes" described in Section 5.5) while the other half are human-verified artifacts.

AUTOSCAN uses 37 high level features to distinguish between real detections and artifacts. The three most important are the ratio of PSF-fitted flux to aperture flux, the magnitude difference between a transient and its nearest static neighbor and the aforementioned SPREAD_MODEL. Each source is given a score between 0 (artifact) and 1 (high-quality detection). Two detections with a score above 0.3 from different images (from different nights and/or different bands) separated by less than $1''$ form a transient candidate. Detections from additional epochs are added to this candidate and analyzed to produce transient light curves and locate likely host galaxies (Kessler et al. 2015), but that process is beyond the scope of this paper.

5.7. *Supernova Image Evaluation*

To evaluate whether a transient is a Type Ia supernova, we must obtain regularly sampled light curves from high quality images. We thus evaluate each supernova image within hours of acquisition to determine if it passes our quality cuts. If any of the g, r, i or z images from the shallow fields fail quality cuts, we resubmit the entire four image sequence for reobservation. The images from the deep fields are evaluated individually (as single-band coadded images), and if any of them fails our quality cut, that single band sequence is retaken.

Images are evaluated via two criteria: depth and image quality. We evaluate depth by obtaining a mean signal to noise ratio of the magnitude 20 fake sources from Section 5.7 in each image (excluding those flagged as being bad detection due to chip gaps, etc.). In shallow fields, these sources must have a signal to noise ratio greater than 20 while in deep fields they must have signal to noise ratio greater than 80. We evaluate the PSF as the mean FWHM of all well-detected fakes. We then estimate what the i-band PSF at zenith as:

$$\mathrm{FWHM_{i,zenith}} = \frac{\mathrm{FWHM}}{\mathrm{K} \times \mathrm{AIRMASS}^{0.6}} \quad (6)$$

where K is the appropriate Kolmogorov coefficient (discussed in Section 4.7) that converts between the observation band and the i band, and the airmass term corrects for the fact that the telescope is not generally pointing at zenith. Supernova fields that do not satisfy $\mathrm{FWHM_{i,zenith}} < 2''$ are sent back to the observing queue to be retaken.

6. MULTI-EPOCH PROCESSING

Coadding exposures to produce deeper images is crucial for most of the DES science goals. We do not repeat the masking, calibration or other image processing described in Sections 3 and 4. We first divide the sky into "coadd tiles" and work with all acceptable exposures within each tile. We optimize the coadds by refining the astrometry from Section 4.1. We then resample the individual exposures, assemble the coadded images, model the coadded PSF and finally create output catalogs. We produce additional files that include pixel-level data and PSF models of every image of every detected source and use the perform optimal photometry and morphology measurements. We discuss coadd production below.

6.1. *Coadd Tiles*

Since we cannot process all DES data at once, we divide the sky into coadd tiles that are rectangular tangent projections. Each tile is $10,000 \times 10,000$ pixels. Each coadded pixel is a $0''263$ square, meaning each tile is $2630''$ or $0.7306°$ on a side. Tiles are arranged along rows of constant declination, with the northernmost row being centered at declination $30°$

and each subsequent row being $0.7138°$ south. This northern declination limit is $25°$ above any DES data, and it allows us to include non-DES DECam data outside the DES area in our database. Each row has a tile centered at right ascension of $275°$ and tiles are spaced by roughly $0.71°$ in angular distance in either direction. There is a roughly $1'$ overlap between tiles, so every source will have a tile in which it is at least $0.'5$ from the edge. The coaddition processes described below use every image (at the individual CCD level) with a given coadd tile.

6.2. *Astrometric Refinement*

Astrometric solutions of overlapping exposures can vary relative to one another. To produce a consistent solution and minimize the width of the coadded PSF, we recalculate our astrometric solutions simultaneously. This requires that we find every image (at the CCD level) in a coadd tile and rerun SCAMP on the images simultaneously.

For each coadd tile we use the Final Cut SEXTRACTOR catalogs for all of the CCDs in all of the exposures that fall within that tile for astrometric remapping. The positions of objects in these catalogs already reflect the Final Cut astrometric solution. We use these catalogs as input for the multi-epoch astrometric refinement step in which we run SCAMP (using the 2MASS stellar catalog as our reference for Y3A2 release) and compute a global astrometric solution for all overlapping exposures using the settings in Appendix D, Table 22. This results in $0.''03$ RMS or better relative astrometry. The proper motion of Milky Way stars and the final registration of the coadd astrometry to 2MASS, from year 1999, compared with DES Y1-Y3, obtained during years 2013-2016, cause an apparent systematic shift of positions in the DES Y3A2 release when compared with Gaia (for example) of up to 350 mas. Future releases (Y5, DR2) will calibrate on the Gaia system to remove this offset. Gaia is a much closer temporal match to DES and will enable relative and absolute measurements of star positions of order $0.''03$ or better.

6.3. *Coadd Image Generation*

Having used SCAMP to recalculate mutually consistent astrometric solutions for the input images, we resample the images so that their pixels are matched to those in our coadd tile. We perform some preprocessing to ensure only good pixels (as described by their pixel flags) are used as inputs into the final coadd. We then use SWARP (Bertin et al. 2002) from the ASTROMATIC package to resample the input images and produce the final coadd images.

Inputs to SWARP are the set of all single-epoch Final Cut images which overlap the tile in question along with a photometric zeropoint for each CCD for each image. These photometric zeropoints come from FGCM described in Section 4.8. The set of single epoch input images actually consists of four planes of data. The first contains on-sky flux (electrons/pixel). Within the coadd pipeline, we linearly interpolate across columns flagged with BPM or TRAIL (but not EDGE) flags to produce contiguous pixels. These interpolated pixels are flagged with the INTERP flag. The second plane is a sixteen-bit mask of bad pixels, cosmic rays, satellite streaks, bleed trails, etc. The third is a weight plane derived from the fitted sky PCA background for that image. We use the mask plane from each input image to ensure that dubious pixels around saturated regions and other image defects are not included in the final coadd. Specifically, we set the weight of pixels with the BADAMP, EDGEBLEED, SSXTALK, EDGE or STREAK flags from Table 9 to zero. In a fourth plane, we also set the weight of the interpolated BPM and TRAIL pixels to zero.

Some data are excluded from coaddition either at the exposure or CCD level (Drlica-Wagner et al. 2017). This "blacklist" of poor data includes CCDs with large scattered light artifacts, spurious excess noise or airplane or meteor streaks. It contains fewer than 1% of CCD images.

We use SWARP and the settings in Appendix D, Table 23 to resample and combine the images into the final coadded image. We run SWARP once with each of the two weight planes described above. We use the first (less masked) weight plane to produce the science image. These images are contiguous across interpolated regions (e.g. bright stars) rather than having zero value in these regions. This is both aesthetically pleasing and prevents sharp edges around masked regions that produce false detections in SEXTRACTOR. We use the SWARP weight output, constructed using the second set of weight images, to produce the final coadded weight image. This ensures that all coadded pixels have the correct weight, particularly that pixels with no valid input pixels have zero weight.

In addition to performing this coaddition on g, r, i, z and Y images separately, we also produce a CHI-MEAN detection image which is a CHI-MEAN coadd of the r, i and z images (Szalay et al. 1999, Drlica-Wagner et al. 2017). We do not include g-band images, because they have larger PSFs and noisy sky backgrounds that would degrade the detection image. In addition, the DES cosmology projects are focused on redder objects. We do not include Y-band images, because they have limited depth and irregular PSFs that would also degrade the detections image. We ultimately run SEXTRACTOR on this detection image to obtain a master list of sources and source shapes.

At this point our coadded images are complete. Fig. 8 shows a $10' \times 4'$ rectangle of sky at varying depths. This particular field overlaps the DES SN-X3 SN field and thus many repeated visits are available to coadd. The top cut combines 4 Final Cut exposures in each of the g, r, i and z bands to produce coadd images with effective exposure time of roughly 360 seconds in each band. The bottom panel uses the supernova coadds of the same area, includes 10-50 times the exposure time, depending on band, and reaches 1-2 magnitudes deeper.

6.4. *Coadded PSF Extraction*

We use PSFEX to produce PSF models for the single-band and detection coadded images using a method similar to that presented in Section 4.5. To produce star catalogs, we run SEXTRACTOR with the same parameters as in the single epoch run (Appendix B, Table 12) except with a more conservative DETECT_THRESH = 5.0. We run SEXTRACTOR with identical parameters to those in Table 13. We also add parameters SAMPLE_WFLAGMASK= 0x0000 and SAMPLE_IMAFLAGMASK= 0x0000.

PSFEX does not model PSFs in coadded images as well as in individual exposures. Each coadd tile is a stack of dithered individual CCDs from different exposures. The discontinuous boundaries at the edge of the input images lead to discontinuities in the PSF that PSFEX does not model. Ultimately, this inaccurate PSF model results in imprecise photometry and morphology measurements from the coadded images. This is not a major issue in the detection image, because it is primarily used to detect objects and not for precise photometry.
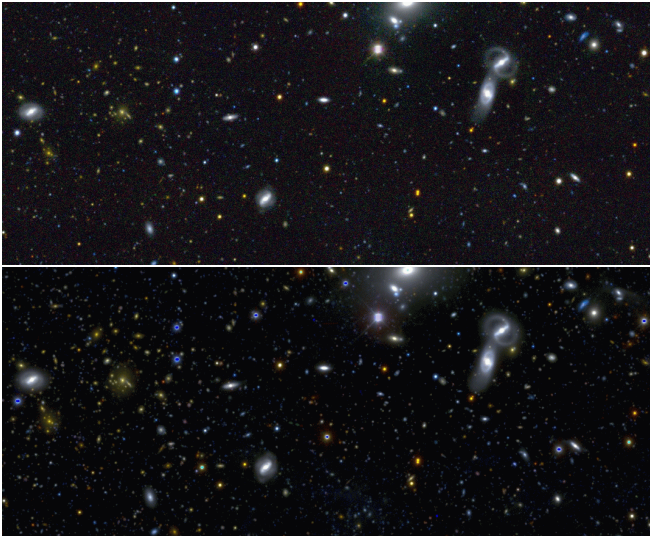
Figure 8. A $10' \times 4'$ subsections of coadd tile DES0227-0458 (the center of the tile is at Right Ascension $02^h 27^m$, Declination $-4°58'$). The RGB channels of the image are the $i+z$ bands, the r band and the g band, respectively. The top panel shows typical 2 year wide-area coadd depth. The bottom panel shows increased depth allow in supernova fields after three years. Saturated pixels appear as blue in the bottom figure.

However, it limits photometric precision in the single-band coadded images. In areas with heterogeneous PSFs, photometric precision can be limited to a few percent. In Section 6.6, we describe the simultaneous fitting of data from all epochs on the sources from the detection images in individual exposures where the PSF can be modeled accurately (Drlica-Wagner et al. 2017).

6.5. *Coadd Catalogs*

We use SEXTRACTOR produce catalogs from the coadded images using the settings in Appendix D, Table 24. We use the $r+i+z$ detection image to find and localize sources with a detection threshold of $S/N \sim 10$. We then run SEXTRACTOR in dual image mode using the using the $r+i+z$ detection image to define the location of the sources and the single-band images to obtain photometry. These catalogs comprise our primary object tables, and we add a series of useful quantities to the objects within them. The catalogs from the DES Y1+Y2+Y3 are comprised of 400 million objects.

The set of parameters measured for every object includes basic flag and position values (FLAGS, ALPHAWIN_J2000_DET, DELTAWIN_J2000_DET), and calibrated photometry (MAG_AUTO and MAG_PSF magnitudes) for every object. Caution should be used with the MAG_PSF quantities due to the heterogeneous nature of the coadd PSF (see Section 6.4). To mitigate the impact of a poor PSF fitting over the coadded images, we provide a set of weighted-mean quantities. These weighted-mean quantities are calculated from single-epoch detections within $1''$ of each object in the coadd detection catalog. Two of the most useful weighted-mean quantities are WAVG_MAG_PSF and WAVG_SPREAD_MODEL.[7] The individual PSF magnitudes are weighted by the inverse statistical uncertainty (with calibration uncertainty added in quadrature) squared. The individual SPREAD_MODEL are weighted by the inverse

SPREADERR_MODEL squared. Unfortunately these mean quantities are only available down to the single-epoch detection limit, which is roughly a magnitude shallower than the coadd. Coadd objects have the IMAFLAGS_ISO parameter set if they contain pixels that have masked bits set in *all* input images. This flag is predominantly set for saturated objects and objects with missing data.

We also run SEXTRACTOR separately on the detection image alone to determine our canonical sky position for each source. We use the model PSFs from Section 6.4. As in Section 4.6, we convolve our images with a 7×7 pixel Gaussian with a 3 pixel FWHM filter as part of the SEXTRACTOR run. Sources in the roughly $30''$ overlap between two tiles (described in Section 6.1) can be multiply detected. In this case we only report the detection closest to a tile center in the catalogs.

We append several "value added" columns to the catalogs. To account for interstellar extinction from dust, we include $E(B-V)$ values from the Schlegel et al. (SFD; 1998) reddening map at the location of each catalog object. The $E(B-V)$ values are obtained using a linear interpolation of the originally distributed map in Lambert polar equal-area projection (i.e., dust_getval.c from Schlegel). The conversion from $E(B-V)$ to an extinction corrected magnitude is an active research topic with DES, and we leave it's derivation to future work (DES Collaboration 2018). While calculating $E(B-V)$ for the catalog, we calculate Galactic coordinates, (l,b), which are included in the final catalog.

We assign each source in the catalog a HEALPix pixel (Górski et al. 2005) using the HEALPY wrapper.[8] This provides simple spatial binning for plotting and statistical angular measurements. We assign each source its pixel value using $\phi = $ RA, $\theta = 90° - $ Dec and nside $= 2^{14} = 16384$. Each HEALPix pixel has an area of roughly 166 arcsec^2.

The above parameters are among the most important in our coadd catalogs, but do not represent an exhaustive list which is available on our public data release website.[9]

6.6. *Data Products for Cosmological Analysis*

At this stage, we have produced final images and detection catalogs for both the single epoch and coadded data. However, additional data products are required for cosmological analyses. We require depth maps, optimal photometry, morphology measurements and photometric redshifts. These data products are not included with DR1, but will be publicly released some time after the main DES data release.

We produce spatial depth maps using the MANGLE code (Swanson et al. 2008, **?**). MANGLE's basic function is to make regions (masks) as a set of covering, disjoint polygons on a spherical surface. These regions carry with them various measures of observing conditions and data quality (e.g. FWHM, exposure time, $t_{\rm eff}$ and other image characteristics). In our processing, MANGLE makes a model for each exposure (working with individual CCD images) using its astrometry information to create the basic outline and previously saved outlines of masked (zero weight) regions of saturated stars, bleed trails and streaks. For a given tile (Section 6.1), MANGLE uses the outlines of all CCDs in the coadded image to form a set of polygons that represent the final coadded image. We use this mask and exposure information to construct maps of depth and related quantities (e.g. limiting magnitude, PSF

---

[7] SPREAD_MODEL is a SEXTRACTOR parameter derived from the Fisher's linear discriminant between a model of the PSF and an extended source model convolved with the PSF (Desai et al. 2012).

[8] http://healpix.sourceforge.net
[9] https://des.ncsa.illinois.edu/releases

and sky variance) at every point in out survey. These quantities are then linked to the final objects catalogs using the object IDs and locations from the coadd catalogs. Our use of MANGLE is described in more detail in Drlica-Wagner et al. (2017).

We also produce Multi Epoch Data Structures (MEDS) for future analysis (Jarvis et al. 2015). MEDS files include image, PSF and catalog information on every object detected in the coadd detection image for each tile. Specifically, they contain postage stamps of the science, weight, mask, background and SEXTRACTOR segmentation map images for each object from both the coadd and all single-epoch images. They also contain models of the local PSFs from PSFEX. We determine the size of each region from the SEXTRACTOR catalog value `FLUX_RADIUS` and round this value up to the next integer multiple of 16 pixels. Typically, this is 32 or 48 pixels. In addition we pass along photometric zeropoints and astrometry information for each object so that a complete analysis can be performed on each object using the MEDS file alone.

We use the output from MEDS to perform multi-epoch, multi-object fitting (MOF) to obtain more robust photometric and morphological measurements of every object Drlica-Wagner et al. (2017). MOF uses the PSF and location information from MEDS to fit a stellar (unresolved PSF) model and a composite galaxy model to every detected object. MOF also addresses the problem of near-neighbor flux contamination by simultaneously fitting groups of sources that have been linked with a friends-of-friends algorithm. We use this MOF photometry as our canonical photometry for all cosmological analyses. It is superior to single-epoch and coadd photometry for most applications.

We measure galaxy ellipticity and ultimately gravitational lensing shear using the Metacalibration method described in Huff & Mandelbaum (2017) and Sheldon & Huff (2017). This method simulates a small shear on the images in the MEDS postage stamps and measures the derivative of ellipticity with respect to shear. This quantity can in turn be robustly related to the underlying gravitational lensing shear.

Finally, we currently derive photometric redshifts for our objects using a template fitting procedure as an afterburner described in some detail in Hoyle et al. (2017). This pipeline step is still under active development.

7. CONCLUSION

This paper has described the pipelines used to process raw DES exposures into science images and catalogs. The processes described here were used through the survey's first three years and its first public data release. DES produces multi-band images with an unprecedented combination of depth, image quality, and area. The DES Collaboration uses this data to probe the history of cosmic expansion and the nature of dark energy using four probes: weak lensing, galaxy clusters, large scale structure and supernova observations. The public release of the DES data will only increase the breadth of scientific investigation.

The development and operation of the DES science pipelines has been central to the success of DES, while also serving as a pathfinder for the next generation of ground-based imaging experiments – i.e., the Large Synoptic Survey Telescope's 10-year survey. The maturation of the DES science pipeline has been driven by two needs. First, the execution of the survey itself, and second, the science needs of the DES Collaboration. These have led directly to the split between First Cut and Final Cut and allows the processing to

be focused toward an immediate goal. In the case of First Cut, the goal is to feedback data quality to the observing team within 24 hours of an observation. For Final Cut the goal is to ensure consistency, uniformity and to maximize the science realizable with any one data release. By keeping the elements within First Cut and Final Cut as similar as possible, we can also use the First Cut processing to 1) help inform what updates to codes and/or calibrations are needed, 2) provide subsequent reprocessing campaigns with data quality assessments to determine which observations should be included in release processing campaigns, and 3) enable early testing of algorithmic improvements at scale. Moreover, because the pipeline products are similar, First Cut and Final Cut products can be combined to enable early scientific analysis of transient phenomena close in time to when the observations occurred.

Many large astronomical surveys develop their own software suites for data processing. Conversely, DES used the ASTROMATIC package (SEXTRACTOR, PSFEX, SCAMP and SWARP) and HOTPANTS for its core processing tasks. After significant experimenting with input parameters and some work with the developer, we found this software performed satisfactorily. Having developed our core software early allowed us to focus on DECam-specific development (e.g. the sky subtraction and masking algorithms) and cosmology code (e.g. MEDS, MOF and Metacalibration) and was essential for developing and end to end survey in a timely manner.

DES originally planned for yearly internal data releases/realizations. By the time the Y1 release occurred it was clear that detailed feedback from the DES Collaboration toward continued improvement of the pipelines would not match that cadence. Thus DES has moved to bi-annual data releases so that improvements based on the scientific analysis could be implemented before the next release was produced.

Underlying the science algorithm improvements in the pipelines is a workflow system that tracks detailed processing (and reprocessing) provenance, processing meta-data, and data quality assessment with enough flexibility to enable integration of changes and new algorithms. The present DESDM workflow and pipeline system, with a development, release, feedback and reprocessing cycle built-in, has served DES well through its internal and public data releases to date. We look forward to carrying out further refinements in the near future to obtain the most out of the extraordinary DES data set.

REFERENCES

Abazajian, K. N., et al. 2009, ApJS, 182, 543
Adelman-McCarthy, J. K., Agüeros, M. A., Allam, S. S., et al. 2007, ApJS, 172, 634
Aihara, H., Arimoto, N., Armstrong, R., et al. 2017, arXiv:1704.05858
Annis, J., et al. 2011, arXiv:1111.6619
Antilogus, P., Astier, P., Doherty, P., Guyonnet, A., & Regnault, N. 2014, Journal of Instrumentation, 9, C03048
Becker, A. 2015, Astrophysics Source Code Library, ascl:1504.004
Benítez, N. 2000, ApJ, 536, 571
Bertin, E., & Arnouts, S. 1996, A&AS, 117, 393
Bertin, E., Mellier, Y., Radovich, M., Missonnier, G., Didelon, P., & Morin, B. 2002, Astronomical Data Analysis Software and Systems XI, 281, 228
Bertin, E. 2006, Astronomical Data Analysis Software and Systems XV, 351, 112
Bertin, E. 2011, Astronomical Data Analysis Software and Systems XX, 442, 435
Bernstein, G., Abbot, T., Gruendl R., et al. 2017, Instrumental response model and detrending for the Dark Energy Camera (In preparation)
Bode B., Butler M., Dunning T., et al. 2013, in Contemporary High Performance Computing From Petascale toward Exascale, ed. Vetter, J. S. (London: Chapman and Hall/CRC), 339
Bramich, D. M., Vidrih, S., Wyrzykowski, L., et al. 2008, MNRAS, 386, 887
Burke, D. L., Rykoff, E. S., Allam, S., et al. 2018, AJ, 155, 41
Calabretta, M. R., & Greisen, E. W. 2002, A&A, 395, 1077
Cardelli, J. A., Clayton, G. C., & Mathis, J. S. 1989, ApJ, 345, 245
Carlstrom, J. E., Ade, P. A. R., Aird, K. A., et al. 2011, PASP, 123, 568
Chadwick, K., Berman, E., Canal, P., et al. 2008, Journal of Physics Conference Series, 119, 052010
Derylo, G., Diehl, H. T., & Estrada, J. 2006, Proc. SPIE, 6276, 627608
Desai, S., Armstrong, R., Mohr, J. J., et al. 2012, ApJ, 757, 83
Desai, S., Mohr, J. J., Bertin, E., Kümmel, M., & Wetzstein, M. 2016, Astronomy and Computing, 16, 67
DES Collaboration, 2005, astro-ph/0510346
DES Collaboration, 2016, MNRAS, 460, 1270
DES Collaboration, 2017, arXiv:1708.01530
DES Collaboration, 2018, in prep.
de Jong, J. T. A., Verdoes Kleijn, G. A., Kuijken, K. H., & Valentijn, E. A. 2013, Experimental Astronomy, 35, 25
Drlica-Wagner et al. 2017, The Dark Energy Survey First Year Cosmology Data Set (In Preparation)
Duda, R., & Hart, P. 1972, J Commun. ACM, 15, 11
Estrada, J., Alvarez, R., Abbott, T., et al. 2010, Proc. SPIE, 7735, 77351R
Fitzpatrick, E. L. 1999, PASP, 111, 63
Fitzpatrick, M. 2010, Astronomical Data Analysis Software and Systems XIX, 434, 260
Flaugher, B., Diehl, H. T., Honscheid, K., et al. 2015, AJ, 150, 150
Freyhammer, L. M., Andersen, M. I., Arentoft, T., Sterken, C., & Nørregaard, P. 2001, Experimental Astronomy, 12, 147
Gaia Collaboration, Brown, A. G. A., Vallenari, A., et al. 2016, A&A, 595, A2
Goldstein, D. A., D'Andrea, C. B., Fischer, J. A., et al. 2015, AJ, 150, 82
Górski, K. M., Hivon, E., Banday, A. J., et al. 2005, ApJ, 622, 759
Gruen, D., Bernstein, G. M., Jarvis, M., et al. 2015, Journal of Instrumentation, 10, C05032
Gruppioni, C., Ciliegi, P., Rowan-Robinson, M., et al. 1999, MNRAS, 305, 297
Hamilton, A. J. S. and Tegmark, M. 2004, MNRAS, 349, 115
Henden, A. A., Welch, D. L., Terrell, D., & Levine, S. E. 2009, American Astronomical Society Meeting Abstracts #214, 214, 407.02
Honscheid, K., Elliott, A., Annis, J. et al. 2012, Proc. SPIE, 8451, 845112
Hoyle, B., Bernstein, G. M., et al. 2017, arXiv:1708.01532
Huff, E., & Mandelbaum, R. 2017, arXiv:1702.02600
Ivezic, Z., Tyson, J. A., Abel, B., et al. 2008, arXiv:0805.2366
Jarvis, M., Sheldon, E., Zuntz, J., et al. 2016, arXiv:1507.05603
Jolliffe, I. T. 1986, Springer Series in Statistics, Berlin: Springer, 1986,
Jurić, M., Kantor, J., Lim, K., et al. 2015, arXiv:1512.07914

Name	Description	Update Frequency	Used By
Header Update	GainAB, ReadnoiseAB, SaturateAB amp keywords	Survey	Crosstalk
Crosstalk Matrix	Matrix of Crosstalk correction between amps/CCDs	Survey	Crosstalk
Brighter-Fatter Correction	Matrix for PSF deconvolution for brighter-fatter effect	Survey	PIXCORRECT
Nonlinearity LUT	Look up table to correct for Non-linearity	Survey	PIXCORRECT
BPM	Bad Pixel Mask	Epoch	PIXCORRECT
Dome Flat	Image of Blanco white spot with DECam	Nightly	PIXCORRECT
Dome Superflat	Average of 50-100 Dome Flats	Epoch	PIXCORRECT
Bias	zero second exposure	Nightly	PIXCORRECT
Biascor Supercal	Average of 50-100 Bias frames	Epoch	PIXCORRECT
TPV Distortion	Estimate of astrometric distortion of each CCD	Epoch	SCAMP
PCA Binned Sky	128x128 binned sky background PCA components	Epoch	Sky Subtraction
PCA Sky Template	Full resolution sky background PCA components	Epoch	Sky Subtraction
Starflat	Multiplicative, large scale (> arcmin) DECam response	Epoch	Sky Subtraction

Table 6
Files used by Preprocessing routines. We present them in the order they are used by the pipeline.

Name	File Path
Header Update	`config/20170531/finalcut/20170531_DES_header_update.20170329`
Crosstalk Matrix	`cal/xtalk/20130606/DECam_20130606.xtalk`
Brighter Fatter Correction	`cal/bf/20170406-r2959/p01/D_n20170406_r2959p01_bf.fits`
Nonlinearity LUT	`cal/lintable/20170314/lin_tbl_v0.7.fits`
BPM	`cal/bpm/20170201t0213-r2927/p01/`
Dome Flat	`precal/20150212-r1402/p01/dflatcor/`
Dome Superflat	`supercal/Y4N/20170201t0213-r2922/p01/norm-dflatcor/`
Bias	`precal/Y4N/20170208-r2923/p01/biascor/`
Biascor Supercal	`supercal/Y4N/20170201t0213-r2922/p01/biascor/`
TPV Distortion	`config/20170531/finalcut/20170531_decam_pvmodel_Y4E2_i.ahead`
PCA Binned Sky	`cal/skytemp/20170103t0315-r2932/p01/binned-fp/`
PCA Sky Template	`cal/skytemp/20170103t0315-r2932/p01/tmpl/`
Starflat	`cal/starflat/20170103t0315-r2933/p01/`

Table 7
Links to samples of files used by Preprocessing routines. These links are all prefaced with `http://data.darkenergysurvey.org/aux/sample/`. In cases where only a directory is given, the directory contains many examples of the file in question, generally one per CCD and/or band.

Kaiser, N., Burgett, W., Chambers, K., et al. 2010, Proc. SPIE, 7733, 77330E
Kessler, R., Bernstein, J. P., Cinabro, D., et al. 2009, PASP, 121, 1028
Kessler, R., Marriner, J., Childress, M., et al. 2015, AJ, 150, 172
Kolmogorov, A. 1941, Akademiia Nauk SSSR Doklady, 30, 301
Krause, E., Eifler, T. F., Zuntz, J., et al. 2017, arXiv:1706.09359
Mohr, J. J., Adams, D., Barkhouse, W., et al. 2008, Proc. SPIE, 7016, 70160L
Mohr, J. J., Armstrong, R., Bertin, E., et al. 2012, Proc. SPIE, 8451, 84510D
Monet, D. G., Levine, S. E., Canzian, B., et al. 2003, AJ, 125, 984
Neilsen, E., & Annis, J. 2013, ObsTac: automated execution of Dark Energy Survey observing tactics, FERMILAB-CONF-13-397-CD
Neilsen, E., Bernstein, G., Gruendl, R., and Kent, S. 2015, Limiting magnitude, τ, T_{eff}, and image quality in DES Year 1, FERMILAB-TM-2610-AE-CD
Ngeow, C., Mohr, J. J., Alam, T., et al. 2006, Proc. SPIE, 6270, 627023
O'Donnell, J. E. 1994, ApJ, 422, 158
Pierre, M., Valtchanov, I., Altieri, B., et al. 2004, J. Cosmology Astropart. Phys., 9, 011
Plazas, A. A., Bernstein, G. M., & Sheldon, E. S. 2014, Journal of Instrumentation, 9, C04001
Roddier, F. 1981, Progress in optics. Volume 19. Amsterdam, North-Holland Publishing Co., 1981, p. 281-376., 19, 281

Schlafly, E. F. & Finkbeiner, D. P. 2011, ApJ, 737, 103
Schlegel, D. J., Finkbeiner, D. P., & Davis, M. 1998, ApJ, 500, 525
Sevilla, I., Armstrong, R., Bertin, E., et al. 2011, arXiv:1109.6741
Sheldon, E. S., & Huff, E. M. 2017, ApJ, 841, 24
Skrutskie, M. F., Cutri, R. M., Stiening, R., et al. 2006, AJ, 131, 1163
Szalay, A. S., Connolly, A. J., & Szokoly, G. P. 1999, AJ, 117, 68
Swanson, M. E. C., Tegmark, M., Hamilton, A. J. S., & Hill, J. C. 2008, MNRAS, 387, 1391
Thain, D., Tannenbaum, T., & and Livny M. 2005, Concurr. Comput. Pract. Exper. 17, 323
Tucker, D. L., Annis, J. T., Lin, H., et al. 2007, The Future of Photometric, Spectrophotometric and Polarimetric Standardization, 364, 187
Xue, Y. Q., Luo, B., Brandt, W. N., et al. 2011, ApJS, 195, 10
York, D. G., Adelman, J., Anderson, J. E., Jr., et al. 2000, AJ, 120, 1579
Zacharias, N., Monet, D. G., Levine, S. E., et al. 2004, Bulletin of the American Astronomical Society, 36, 48.15
Zacharias, N., Finch, C. T., Girard, T. M., et al. 2013, AJ, 145, 44
Zuntz, J., Sheldon, E., Samuroff, S., et al. 2017, arXiv:1708.01533

APPENDIX

APPENDIX A: INPUT FILE AND FLAG DESCRIPTIONS

In Section 3, we describe input files and two sets of flags which we tabulate below. Table 6 describes the input files we use in Preprocessing, and Table 7 gives links to example files. Table 8 shows the Bad Pixel Mask (BPM) flags. These flags are applied to BPM images that are generated once for each set of calibration images, which are in turn remade every time the camera warms up (typically twice per year).

Table 9 shows the bitmask flags. These are generated for each individual exposure. Some flags are derived from the BPM and are constant for every exposure in an epoch. Others mark the saturated regions, cosmic rays, streaks and other defects in individual exposures.

BPM Name	Value	Hex	Description
BPMDEF_FLAT_MIN	1	0x0001	Flat pixel < 50% mean
BPMDEF_FLAT_MAX	2	0x0002	Flat pixel > 150% mean
BPMDEF_BIAS_HOT	8	0x0008	Bias pixel > 500 counts
BPMDEF_BIAS_WARM	16	0x0010	Bias pixel > 20 counts
BPMDEF_BIAS_COL	64	0x0040	Downstream (in readout order) from hot pixel
BPMDEF_EDGE	128	0x0080	Nearest 15 pixels to the CCD edge
BPMDEF_SUSPECT	512	0x0200	Regions with small, non-quantifiable errors (See text)
BPMDEF_FUNKY_COL	1024	0x0400	Columns with anomalous sky values
BPMDEF_WACKY_PIX	2048	0x0800	Areas with anomalous sky values
BPMDEF_BADAMP	4096	0x1000	Unusable amplifier (right amp of DECam CCD 31)
BPMDEF_NEAREDGE	8192	0x2000	25 edge columns unreliable on 1-2% level
BPMDEF_TAPEBUMP	16384	0x4000	Each CCD has 6 tape bumps (See text)

Table 8
Bad Pixel Mask (BPM) bit descriptions. Values are listed as conventional integers and in hexadecimal.

Bitmask Name	Value	Hex	Description
BADPIX_BPM	1	0x0001	BPM value 0x0c5b (see exceptions in text)
BADPIX_SATURATE	2	0x0002	Pixel above amplifier's saturation value in debiased image
BADPIX_INTERP	4	0x0004	Pixel whose value was interpolated from neighbors
BADPIX_BADAMP	8	0x0008	Identical to BPMDEF_BADAMP (BPM=0x1000)
BADPIX_CRAY	16	0x0010	Pixel contaminated by a cosmic ray
BADPIX_STAR	32	0x0020	Circular mask around bright stars
BADPIX_TRAIL	64	0x0040	Bleed trails form in column with saturated pixels
BADPIX_EDGEBLEED	128	0x0080	Near CCD edges, bleed trails can spread to adjacent pixels
BADPIX_SSXTALK	256	0x0100	Cross talk from saturated pixels is uncertain (though typically small)
BADPIX_EDGE	512	0x0200	Identical to BPMDEF_EDGE (BPM= 0x0080)
BADPIX_STREAK	1024	0x0400	Streak detected
BADPIX_SUSPECT	2048	0x0800	Identical to BPMDEF_SUSPECT (BPM= 0x0200)
BADPIX_FIXED	4096	0x1000	Fixed column with BPMDEF_BIAS_COL or BPMDEF_FUNKY_COL
BADPIX_NEAREDGE	8129	0x2000	Identical to BPMDEF_NEAREDGE (BPM=0x2000)
BADPIX_TAPEBUMP	16384	0x4000	Identical to BPMDEF_TAPEBUMP (BPM=0x4000)

Table 9
Bitmask descriptions for individual flag images. Values are listed as conventional integers and in hexadecimal.

APPENDIX B: SOFTWARE SETTINGS FOR THE FIRST CUT AND FINAL CUT PIPELINES

Tables 10 through 14 are used in First Cut (Section 4) and Final Cut (Section 4.8) processing. Tables 10 and 11 describe the SEXTRACTOR settings used to produce a star catalog for SCAMP and the corresponding SCAMP settings (see Section 4.1). Similarly, Tables 12 and 13 describe the SEXTRACTOR settings used to produce a star catalog for PSFEX and the corresponding PSFEX settings (see Section 4.5). Finally, the SEXTRACTOR settings for our First Cut and Final Cut source catalogs are listed in Table 14.

APPENDIX C: SOFTWARE SETTINGS FOR THE SUPERNOVA PIPELINE

The DES Supernova pipeline (Section 5) has settings independent of the main pipeline that we describe in Tables 15 through 21. Tables 15 and 16 describe the SCAMP settings used to perform the astrometric refinement used for DES difference imaging. The settings in Tables 17 and 18 are used to model the PSF with PSFEx. The supernova pipeline then astrometrically resamples the First Cut-processed image using SWARP and the settings in Table 19. We produce a difference image using HOTPANTS and the settings in Table 20, and use SEXTRACTOR and the settings in 21 to produce an initial catalog of potential transients.

APPENDIX D: SOFTWARE SETTINGS FOR MULTI-EPOCH PROCESSING

Section 6 describes our Multi-Epoch Pipeline in which we coadd processed images to make deeper stacked images. We use SCAMP and the settings in Table 22 to refine the astrometric solutions of our input images in one mutually-consistent solution. We then combine the images into single-band coadds and $r+i+z$ detection images with SWARP (Table 23 and produce single-band and detection catalogs using SEXTRACTOR (Table 24). Due to the difficulties in modeling coadded PSFs, these catalogs are not used for our more precise analysis (see Section 6.6 for MOF description).

Parameter	Value
DETECT_MINAREA	5
DETECT_THRESH	10
ANALYSIS_THRESH	1.5
WEIGHT_THRESH	10^{-5}
FILTER	Y
FILTER_NAME	*See text*
DEBLEND_NTHRESH	32
DEBLEND_MINCONT	0.1
CLEAN	Y
CLEAN_PARAM	1.0
MASK_TYPE	CORRECT
INTERP_TYPE	ALL
INTERP_MAXXLAG	4
INTERP_MAXYLAG	4
SEEING_FWHM	1.2"
STARNNW_NAME	DEFAULT
RESCALE_WEIGHTS	N
BACK_SIZE	256
BACK_FILTERSIZE	3
BACKPHOTO_TYPE	GLOBAL
PSF_NMAX	1
BACK_TYPE	AUTO

Table 10
SEXTRACTOR parameters for SCAMP analysis.

Parameter	Value
FGROUP_RADIUS	3.0
ASTREF_CATALOG	2MASS
ASTREF_BAND	DEFAULT
ASTREFCENT_KEYS	X_WORLD,Y_WORLD
ASTREFERR_KEYS	ERRA_WORLD, ERRTHETA_WORLD
ASTREFMAG_KEY	MAG
MATCH	Y
MATCH_NMAX	0
PIXSCALE_MAXERR	1.2
POSANGLE_MAXERR	5.0
POSITION_MAXERR	10.0
MATCH_RESOL	0
MATCH_FLIPPED	N
MOSAIC_TYPE	SAME_CRVAL
FIXFOCALPLANE_NMIN	1
CROSSID_RADIUS	2.0
SOLVE_ASTROM	Y
ASTRINSTRU_KEY	FILTER,QRUNID
STABILITY_TYPE	INSTRUMENT
CENTROID_KEYS	XWIN_IMAGE, YWIN_IMAGE
CENTROIDERR_KEYS	ERRAWIN_IMAGE, ERRBWIN_IMAGE, ERRTHETAWIN_IMAGE
DISTORT_KEYS	XWIN_IMAGE, YWIN_IMAGE
DISTORT_GROUPS	1,1
DISTORT_DEGREES	3
FOCDISTORT_DEGREE	2
ASTREF_WEIGHT	1.0
ASTRCLIP_NSIGMA	3.0
CORRECT_COLOURSHIFTS	N
SOLVE_PHOTOM	Y
MAGZERO_OUT	0.0
MAGZERO_INTERR	0.01
MAGZERO_REFERR	0.03
ASTREFMAG_LIMITS	$-99, 17$
PHOTCLIP_NSIGMA	3.0
SN_THRESHOLDS	$10.0, 100.0$
FWHM_THRESHOLDS	$0.0, 50.0$
FLAGS_MASK	$0x00f0$
WEIGHTFLAGS_MASK	$0x00ff$
IMAFLAGS_MASK	$0x0000$

Table 11
First Cut SCAMP settings.

Parameter	Value
DETECT_MINAREA	3
DETECT_THRESH	3.0
ANALYSIS_THRESH	1.5
FILTER	Y
FILTER_NAME	all-ground
DEBLEND_NTHRESH	32
DEBLEND_MINCONT	0.005
CLEAN	Y
CLEAN_PARAM	1.0
MASK_TYPE	CORRECT
PSF_NMAX	1
STARNNW_NAME	DEFAULT
RESCALE_WEIGHTS	N
BACK_SIZE	256
BACK_FILTERSIZE	3
BACKPHOTO_TYPE	GLOBAL
RESCALE_WEIGHTS	N
BACK_TYPE	AUTO

Table 12
SEXTRACTOR parameters used to create the catalog for PSFEX analysis.

Parameter	Value
BASIS_TYPE	PIXEL_AUTO
BASIS_NUMBER	20
BASIS_SCALE	1.0
NEWBASIS_TYPE	NONE
NEWBASIS_NUMBER	8
PSF_SAMPLING	0.0
PSF_PIXELSIZE	1.0
PSF_ACCURACY	0.01
PSF_SIZE	25, 25
CENTER_KEYS	X_IMAGE, Y_IMAGE
PSF_RECENTER	N
PHOTFLUX_KEY	FLUX_APER(7)
PHOTFLUXERR_KEY	FLUXERR_APER(7)
MEF_TYPE	INDEPENDENT
PSFVAR_KEYS	X_IMAGE, Y_IMAGE
PSFVAR_GROUPS	1, 1
PSFVAR_DEGREES	2
PSFVAR_NSNAP	9
HIDDENMEF_TYPE	COMMON
STABILITY_TYPE	PRE-DISTORTED
SAMPLE_AUTOSELECT	Y
SAMPLEVAR_TYPE	SEEING
SAMPLE_FWHMRANGE	2.0, 30.0
SAMPLE_VARIABILITY	0.2
SAMPLE_MINSN	20
SAMPLE_MAXELLIP	0.3
SAMPLE_FLAGMASK	$0x00fe$
BADPIXEL_FILTER	N
BADPIXEL_NMAX	0
HOMOBASIS_TYPE	None
HOMOBASIS_NUMBER	10
HOMOBASIS_SCALE	1.0
HOMOPSF_PARAMS	2.0, 3.0
CHECKPLOT_DEV	NULL
CHECKPLOT_RES	0
CHECKPLOT_ANTIALIAS	Y

Table 13
PSFEX parameters used for measuring and modeling DES PSFs.

Parameter	Value
DETECT_MINAREA	6
DETECT_THRESH	1.5
ANALYSIS_THRESH	1.5
FILTER	Y
FILTER_NAME	all-ground
DEBLEND_NTHRESH	32
DEBLEND_MINCONT	0.005
CLEAN	Y
CLEAN_PARAM	1.0
MASK_TYPE	CORRECT
PSF_NMAX	1
STARNNW_NAME	DEFAULT
RESCALE_WEIGHTS	N
BACK_SIZE	256
BACK_FILTERSIZE	3
BACKPHOTO_TYPE	GLOBAL
BACK_TYPE	AUTO
INTERP_TYPE	VAR_ONLY
INTERP_MAXXLAG	4
INTERP_MAXYLAG	4

Table 14
SEXTRACTOR parameters for DES First Cut catalog production.

Parameter	Value
DETECT_MINAREA	3
DETECT_THRESH	5
ANALYSIS_THRESH	5
FILTER	Y
FILTER_NAME	all-ground
DEBLEND_MINCONT	0.05
WEIGHT_TYPE	MAP_WEIGHT
WEIGHT_GAIN	Y
WEIGHT_THRESH	$1.e-10$
PHOT_APERTURES	10
PHOT_AUTOPARAMS	3.5, 3.5
SATUR_LEVEL	15000.0
GAIN	1.0
INTERP_TYPE	NONE

Table 15
SEXTRACTOR settings for catalogs used in the astrometric refinement in the supernova pipeline.

Parameter	Value
FGROUP_RADIUS	1.0
ASTREF_CATALOG	See text
ASTREF_BAND	DEFAULT
ASTREFCENT_KEYS	X_WORLD, Y_WORLD
ASTREFERR_KEYS	ERRA_WORLD, ERRB_WORLD
	ERRTHETA_WORLD
ASTREFMAG_KEY	MAG
MATCH	N
PIXSCALE_MAXERR	1.1
POSANGLE_MAXERR	1.0
POSITION_MAXERR	0.2
MATCH_RESOL	0
MATCH_FLIPPED	N
MOSAIC_TYPE	UNCHANGED
FIXFOCALPLANE_NMIN	1
CROSSID_RADIUS	5.0
SOLVE_ASTROM	Y
PROJECTION_TYPE	TAN
ASTRINSTRU_KEY	FILTER
STABILITY_TYPE	INSTRUMENT
CENTROID_KEYS	XWIN_IMAGE, YWIN_IMAGE
CENTROIDERR_KEYS	ERRAWIN_IMAGE, ERRBWIN_IMAGE
	ERRTHETAWIN_IMAGE
DISTORT_KEYS	XWIN_IMAGE, YWIN_IMAGE
DISTORT_GROUPS	1, 1
DISTORT_DEGREES	1
FOCDISTORT_DEGREE	1
ASTREF_WEIGHT	1.0
ASTRACCURACY_TYPE	SIGMA-PIXEL
ASTRACCURACY_KEY	ASTRACCU
ASTR_ACCURACY	0.01
ASTRCLIP_NSIGMA	3.0
CORRECT_COLOURSHIFTS	N
SOLVE_PHOTOM	Y
MAGZERO_OUT	0.0
MAGZERO_INTERR	0.01
MAGZERO_REFERR	0.03
ASTREFMAG_LIMITS	$-99.0, 99.0$
PHOTCLIP_NSIGMA	3.0
PHOT_ACCURACY	10^{-3}
SN_THRESHOLDS	10.0, 100.0
FWHM_THRESHOLDS	1.0, 20.0
ELLIPTICITY_MAX	0.4
FLAGS_MASK	$0x00ff$
WEIGHTFLAGS_MASK	$0x00ff$
IMAFLAGS_MASK	$0x000$

Table 16
Our SCAMP settings for astrometric refinement in the supernova pipeline.

Parameter	Value
ASSOCCOORD_TYPE	WORLD
ASSOC_RADIUS	2.0
ASSOC_TYPE	NEAREST
ASSOCSELEC_TYPE	MATCHED
DETECT_MINAREA	3
DETECT_THRESH	5
ANALYSIS_THRESH	5
FILTER	Y
FILTER_NAME	all-ground
DEBLEND_MINCONT	0.05
WEIGHT_TYPE	MAP_WEIGHT
WEIGHT_GAIN	Y
WEIGHT_THRESH	10^{-10}
PHOT_APERTURES	10
PHOT_AUTOPARAMS	3.5, 3.5
SATUR_LEVEL	15000.0

Table 17
SEXTRACTOR parameters used to create catalogs for supernova PSFEX analysis.

Parameter	Value
BASIS_TYPE	PIXEL_AUTO
BASIS_NUMBER	16
PSF_SAMPLING	0.7
PSF_ACCURACY	0.01
PSF_SIZE	51, 51
PSF_RECENTER	Y
PSFVAR_KEYS	X_IMAGE, Y_IMAGE
PSFVAR_GROUPS	1, 1
PSFVAR_DEGREES	1
SAMPLE_AUTOSELECT	Y
SAMPLEVAR_TYPE	SEEING
SAMPLE_FWHMRANGE	3.0, 20.0
SAMPLE_VARIABILITY	0.2
SAMPLE_MINSN	20
SAMPLE_MAXELLIP	0.3
CHECKPLOT_DEV	NULL
CHECKPLOT_TYPE	NONE
CHECKPLOT_NAME	fwhm, ellipticity
CHECKIMAGE_TYPE	NONE

Table 18
PSFEX parameters used for measuring and modeling DES PSFs in the supernova fields.

Parameter	Value
COMBINE	Y
COMBINE_TYPE	AVERAGE
BLANK_BADPIXELS	N
CELESTIAL_TYPE	NATIVE
PROJECTION_TYPE	TAN
PROJECTION_ERR	0.001
CENTER_TYPE	ALL
PIXELSCALE_TYPE	MEDIAN
PIXEL_SCALE	0.0
IMAGE_SIZE	0
RESAMPLE	Y
RESAMPLING_TYPE	LANCZOS4
OVERSAMPLING	0
INTERPOLATE	N
FSCALASTRO_TYPE	NONE
FSCALE_KEYWORD	NOTSCALE
FSCALE_DEFAULT	1.0
SUBTRACT_BACK	Y
BACK_TYPE	AUTO
BACK_DEFAULT	0.0
BACK_SIZE	128
BACK_FILTERSIZE	3
BACK_FILTTHRESH	0.0

Table 19
SWARP parameters for matching supernova templates to single epoch science images.

Parameter	Value
useWeight	True
nsx	10
nsy	20
n	t
convvar	True
r	20
rss	25
kfm	0.999
bgo	2
rk0	9.01
wk0	9
wkX	5
wkY	5
rkx	5.01
rky	5.01
ng	116.0
v	1
mcs	10.0
mds	5.0
mdf	0.2
mks	0.05
mnor	5.0
sdif	5.0
serr	10^{-6}
il	-999999
iu	999999
tl	-999999
tu	999999

Table 20
HOTPANTS parameters for photometrically matching supernova template images to nightly science images and producing the resulting difference images.

Parameter	Value
DETECT_MINAREA	1
DETECT_THRESH	1.2
ANALYSIS_THRESH	5.0
FILTER	Y
FILTER_NAME	See text
DEBLEND_NTHRESH	32
DEBLEND_MINCONT	0.005
CLEAN_PARAM	1.0
MASK_TYPE	CORRECT
WEIGHT_TYPE	MAP_WEIGHT
WEIGHT_GAIN	N
WEIGHT_THRESH	$1.e-10$
PHOT_APERTURES	5
PHOT_AUTOPARAMS	$2.5, 3.5$
PHOT_PETROPARAMS	$2.0, 3.5$
SATUR_LEVEL	50000.0
MAG_ZEROPOINT	31.1928
PIXEL_SCALE	1.0
SEEING_FWHM	1.2
BACK_SIZE	64
BACK_FILTERSIZE	3
BACKPHOTO_TYPE	GLOBAL
CHECKIMAGE_TYPE	NONE
INTERP_MAXXLAG	16
INTERP_MAXYLAG	16
INTERP_TYPE	NONE

Table 21
SEXTRACTOR parameters for detecting sources in difference images.

Parameter	Value
FGROUP_RADIUS	3.0
ASTREF_CATALOG	2MASS
ASTREF_BAND	DEFAULT
ASTREFMAG_LIMITS	$-99, 99$
DGEOMAP_STEP	2
DGEOMAP_NNEAREST	21
MATCH	Y
MATCH_NMAX	0
PIXSCALE_MAXERR	1.2
POSANGLE_MAXERR	0.25
POSITION_MAXERR	2.0
MATCH_RESOL	0
MATCH_FLIPPED	N
MOSAIC_TYPE	SAME_CRVAL
FIXFOCALPLANE_NMIN	1
CROSSID_RADIUS	2.0
SOLVE_ASTROM	Y
PROJECTION_TYPE	SAME
STABILITY_TYPE	INSTRUMENT
DISTORT_GROUPS	$1, 1$
DISTORT_DEGREES	3
FOCDISTORT_DEGREE	3
ASTREF_WEIGHT	1.0
ASTRACCURACY_TYPE	SIGMA-PIXEL
ASTR_ACCURACY	0.01
ASTRCLIP_NSIGMA	3.0
COMPUTE_PARALLAXES	N
COMPUTE_PROPERMOTIONS	N
CORRECT_COLOURSHIFTS	N
INCLUDE_ASTREFCATALOG	Y
ASTR_FLAGSMASK	$0x0000$
ASTR_IMAFLAGSMASK	$0x000$
SOLVE_PHOTOM	N
MAGZERO_OUT	0.0
MAGZERO_INTERR	0.01
MAGZERO_REFERR	0.03
PHOTCLIP_NSIGMA	3.0
PHOT_ACCURACY	10^{-3}
PHOT_FLAGSMASK	$0x00fc$
PHOT_IMAFLAGSMASK	$0x0000$
CHECKPLOT_DEV	PSC
CHECKPLOT_RES	0
CHECKPLOT_ANTIALIAS	N
CHECKPLOT_TYPE	FGROUPS,DISTORTION,
	ASTR_REFERROR2D,ASTR_REFERROR1D,
	ASTR_INTERROR2D,ASTR_INTERROR1D,
	ASTR_REFSYSMAP
CHECKPLOT_NAME	fgroups,distortion,
	astr_referror2d,astr_referror1d,
	astr_interror1d,astr_interror2d,
	astr_refsysmap
SN_THRESHOLDS	10.0, 100.0
FWHM_THRESHOLDS	1.0, 10.0
ELLIPTICITY_MAX	0.5
FLAGS_MASK	$0x00fd$
WEIGHTFLAGS_MASK	$0x0000$
IMAFLAGS_MASK	$0x0700$
HEADER_TYPE	NORMAL

Table 22
Multi-Epoch coadd SCAMP settings.

Parameter	Value
HEADER_ONLY	N
WEIGHT_TYPE	MAP_WEIGHT
RESCALE_WEIGHTS	N
COMBINE	Y
COMBINE_TYPE	WEIGHTED/CHI-MEAN
CLIP_AMPFRAC	0.3
CLIP_SIGMA	4.0
CLIP_WRITELOG	N
BLANK_BADPIXELS	N
CELESTIAL_TYPE	NATIVE
PROJECTION_TYPE	TAN
PROJECTION_ERR	0.001
CENTER_TYPE	MANUAL
PIXELSCALE_TYPE	MANUAL
PIXEL_SCALE	0.263
IMAGE_SIZE	10000, 10000
RESAMPLE	Y
RESAMPLING_TYPE	LANCZOS3
OVERSAMPLING	0
INTERPOLATE	N
FSCALASTRO_TYPE	VARIABLE
FSCALE_KEYWORD	nokey
FSCALE_DEFAULT	1.0
SATLEV_DEFAULT	50000.0
SUBTRACT_BACK	Y
BACK_TYPE	AUTO
BACK_DEFAULT	0.0
BACK_SIZE	256
BACK_FILTERSIZE	3
BACK_FILTTHRESH	0.0
COPY_KEYWORDS	BUNIT,FILTER,BAND,TILENAME,TILEID

Table 23
Multi-Epoch coadd SWARP settings. COMBINE_TYPE is WEIGHTED for single-band images and CHI-MEAN for detection images.

MORGANSON ET AL.

Parameter	Value
DETECT_TYPE	CCD
DETECT_MINAREA	4
DETECT_MAXAREA	0
THRESH_TYPE	RELATIVE
DETECT_THRESH	1.1
ANALYSIS_THRESH	1.1
FILTER	Y
FILTER_NAME	*See text*
DEBLEND_NTHRESH	32
DEBLEND_MINCONT	0.001
CLEAN	Y
CLEAN_PARAM	1.0
THRESH_TYPE	RELATIVE
MASK_TYPE	CORRECT
WEIGHT_TYPE	MAP_WEIGHT
RESCALE_WEIGHTS	N
WEIGHT_GAIN	Y
FLAG_TYPE	OR
PHOT_APERTURES	$1.85, 3.70, 5.55, 7.41,$ $11.11, 14.81, 18.52,$ $22.22, 25.93, 29.63,$ $44.44, 66.67$
PHOT_AUTOPARAMS	$2.5, 3.5$
PHOT_PETROPARAMS	$2.0, 3.5$
PHOT_AUTOAPERS	$0.0, 7.41$
PHOT_FLUXFRAC	0.5
GAIN	0.0
PIXEL_SCALE	0
SEEING_FWHM	0
BACK_TYPE	AUTO
BACK_VALUE	0.0
BACK_SIZE	256
BACK_FILTERSIZE	3
BACKPHOTO_TYPE	GLOBAL
BACKPHOTO_THICK	24
BACK_FILTTHRESH	0.0
ASSOC_DATA	$2, 3, 4$
ASSOC_PARAMS	$2, 3, 4$
ASSOCCOORD_TYPE	PIXEL
ASSOC_RADIUS	2.0
ASSOC_TYPE	NEAREST
ASSOCSELECT_TYPE	MATCHED
VERBOSE_TYPE	NORMAL
FITS_UNSIGNED	N
INTERP_MAXXLAG	4
INTERP_MAXYLAG	4
INTERP_TYPE	VAR_ONLY
PSF_NMAX	1
PATTERN_TYPE	RINGS-HARMONIC

Table 24
Our multiepoch coadd SEXTRACTOR settings.